Nut Directs p300-Dependent, Genome-Wide H4 Hyperacetylation in Male Germ Cells

Hitoshi Shiota, Sophie Barral, Thierry Buchou, Minjia Tan, Yohann Couté, Guillaume Charbonnier, Nicolas Reynoird, Fayçal Boussouar, Matthieu Gérard, Mingrui Zhu, et al.

Article

Cell Reports

Nut Directs p300-Dependent, Genome-Wide H4 Hyperacetylation in Male Germ Cells

Graphical Abstract

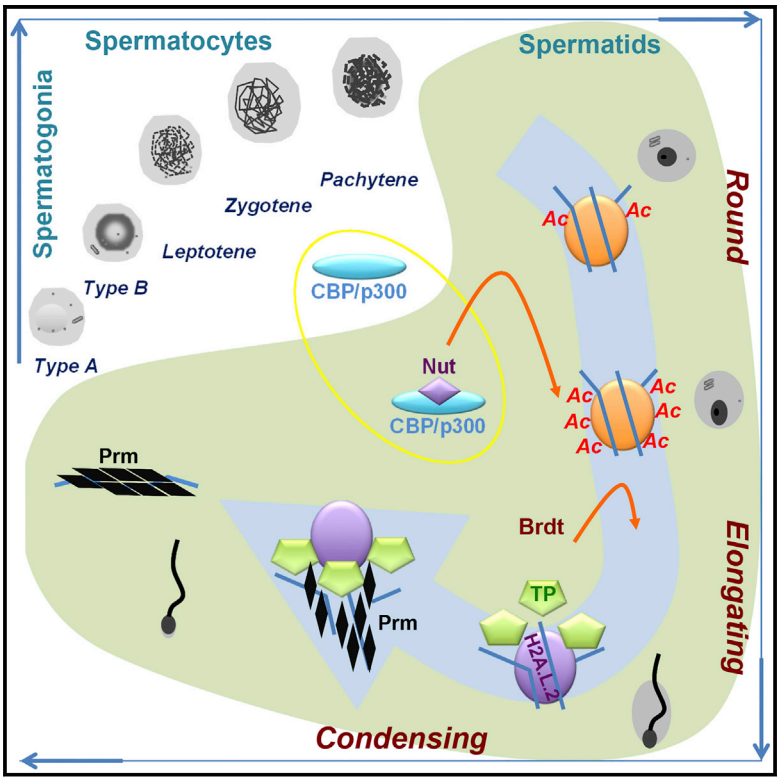

Authors

Hitoshi Shiota, Sophie Barral, Thierry Buchou, ..., Sophie Rousseaux, Yingming Zhao, Saadi Khochbin

Correspondence

saadi.khochbin@univ-grenoble-alpes.fr

In Brief

A transcription-independent histone hyperacetylation is associated with near-total histone replacement during mouse spermatogenesis. Shiota et al. show the oncogenic factor Nut is expressed in post-meiotic male germ cells, where it recruits p300 and/or CBP and enhances histone H4K5 and H4K8 acetylation, leading to histone-to-protamine replacement.

Highlights

- *Nut* is a post-meiotically expressed gene that is critical for male fertility
- Nut recruits p300 and/or CBP to enhance histone H4K5 and H4K8 acetylation
- Nut-mediated histone hyperacetylation is required for histone-to-protamine transition

Data Resources

GSE111931
GSE118969
PXD008727

Shiota et al., 2018, Cell Reports *24*, 3477–3487
September 25, 2018
https://doi.org/10.1016/j.celrep.2018.08.069

CellPress

Cell Reports
Article

Nut Directs p300-Dependent, Genome-Wide H4 Hyperacetylation in Male Germ Cells

Hitoshi Shiota,[1,10] Sophie Barral,[1,10] Thierry Buchou,[1,10] Minjia Tan,[2] Yohann Couté,[3] Guillaume Charbonnier,[4] Nicolas Reynoird,[1] Fayçal Boussouar,[1] Matthieu Gérard,[5] Mingrui Zhu,[2] Lisa Bargier,[4] Denis Puthier,[4] Florent Chuffart,[1] Ekaterina Bourova-Flin,[1] Sarah Picaud,[6] Panagis Filippakopoulos,[6] Afsaneh Goudarzi,[1] Ziad Ibrahim,[7] Daniel Panne,[7,8] Sophie Rousseaux,[1] Yingming Zhao,[9] and Saadi Khochbin[1,11,*]

[1]CNRS UMR 5309, Inserm U1209, Université Grenoble Alpes, Institute for Advanced Biosciences, Grenoble 38700, France
[2]Shanghai Institute of Materia Medica, Chinese Academy of Sciences, 555 Zuchongzhi Road, Shanghai 201203, P.R. China
[3]Université Grenoble Alpes, CEA, Inserm U1038, CEA, BIG-BGE, Grenoble 38000, France
[4]TGML, platform IbiSA, Aix Marseille Université, Inserm U1090, TAGC, Marseille, France
[5]CEA, iBiTec-S, Gif-sur-Yvette 91191, France
[6]Structural Genomics Consortium & Ludwig Institute for Cancer Research, Old Road Campus Research Building, Roosevelt Drive, Oxford OX3 7DQ, UK
[7]EMBL Grenoble, BP 181, 71 Avenue des Martyrs, 38042 Grenoble Cedex 9, France
[8]Leicester Institute of Structural and Chemical Biology, Department of Molecular and Cell Biology, University of Leicester, Lancaster Road, Leicester LE1 7RH, UK
[9]Ben May Department of Cancer Research, The University of Chicago, Chicago, IL 60637, USA
[10]These authors contributed equally
[11]Lead Contact
*Correspondence: saadi.khochbin@univ-grenoble-alpes.fr
https://doi.org/10.1016/j.celrep.2018.08.069

SUMMARY

Nuclear protein in testis (Nut) is a universal oncogenic driver in the highly aggressive NUT midline carcinoma, whose physiological function in male germ cells has been unclear. Here we show that expression of Nut is normally restricted to post-meiotic spermatogenic cells, where its presence triggers p300-dependent genome-wide histone H4 hyperacetylation, which is essential for the completion of histone-to-protamine exchange. Accordingly, the inactivation of *Nut* induces male sterility with spermatogenesis arrest at the histone-removal stage. Nut uses p300 and/or CBP to enhance acetylation of H4 at both K5 and K8, providing binding sites for the first bromodomain of Brdt, the testis-specific member of the BET family, which subsequently mediates genome-wide histone removal. Altogether, our data reveal the detailed molecular basis of the global histone hyperacetylation wave, which occurs before the final compaction of the male genome.

INTRODUCTION

In mammals, unique physiological, genome-wide histone hyperacetylation has been observed, associated with a near-total histone eviction that occurs during the late stages of spermatogenesis. In this context, an outstanding issue is the understanding of the causes and consequences of this histone hyperacetylation and, more precisely, of its role in histone eviction (Goudarzi et al., 2014). After meiosis, haploid cells, named spermatids, engage in one of the most dramatic known chromatin remodeling and genome reorganization processes, which essentially takes place in cells known as elongating and condensing spermatids. It consists of the genome-wide removal of histones and their replacement by small basic proteins, transition proteins (TPs) and protamines (Prms) (Barral et al., 2017; Gaucher et al., 2010). Spermatids are produced following two successive meiotic divisions of spermatocytes, which are continuously generated from the progenitor cells known as spermatogonia.

During the past decades, we have developed strategies to discover the molecular basis of this genome-wide histone hyperacetylation taking place in late haploid male germ cells (Goudarzi et al., 2014). These strategies included a series of structural and functional studies of the testis-specific bromodomain-containing BET factor Brdt. These investigations showed that Brdt's first bromodomain specifically recognizes histone H4 bearing the simultaneous acetylation of K5 and K8 (Goudarzi et al., 2016; Miller et al., 2016; Morinière et al., 2009; Sasaki et al., 2009) and somehow mediates the eviction of histones (Gaucher et al., 2012).

In the frame of these studies, we also became interested in a testis-specific gene of unknown function, nuclear protein in testis (*NUT*), which is involved in a cancer known as NUT midline carcinoma (NMC). NMC is characterized by a series of chromosomal translocations that fuse the *NUT* gene located on chromosome 15q14 to partner genes, most frequently one of the double bromodomain proteins of the BET family, *BRD4* (67% of cases) or *BRD3* (25% of cases). Therefore, in more than 90% of NMC cases, NUT is fused to a double bromodomain BET factor (French, 2012).

Because of the testis-specific nature of *NUT* expression and its cooperation with somatic members of BETs, BRD3 and BRD4 in NMC, we hypothesized that a possible cooperation between NUT and BRDT in the physiological setting of spermatogenesis could occur and be involved in the establishment and management of histone hyperacetylation. Molecular investigations of the

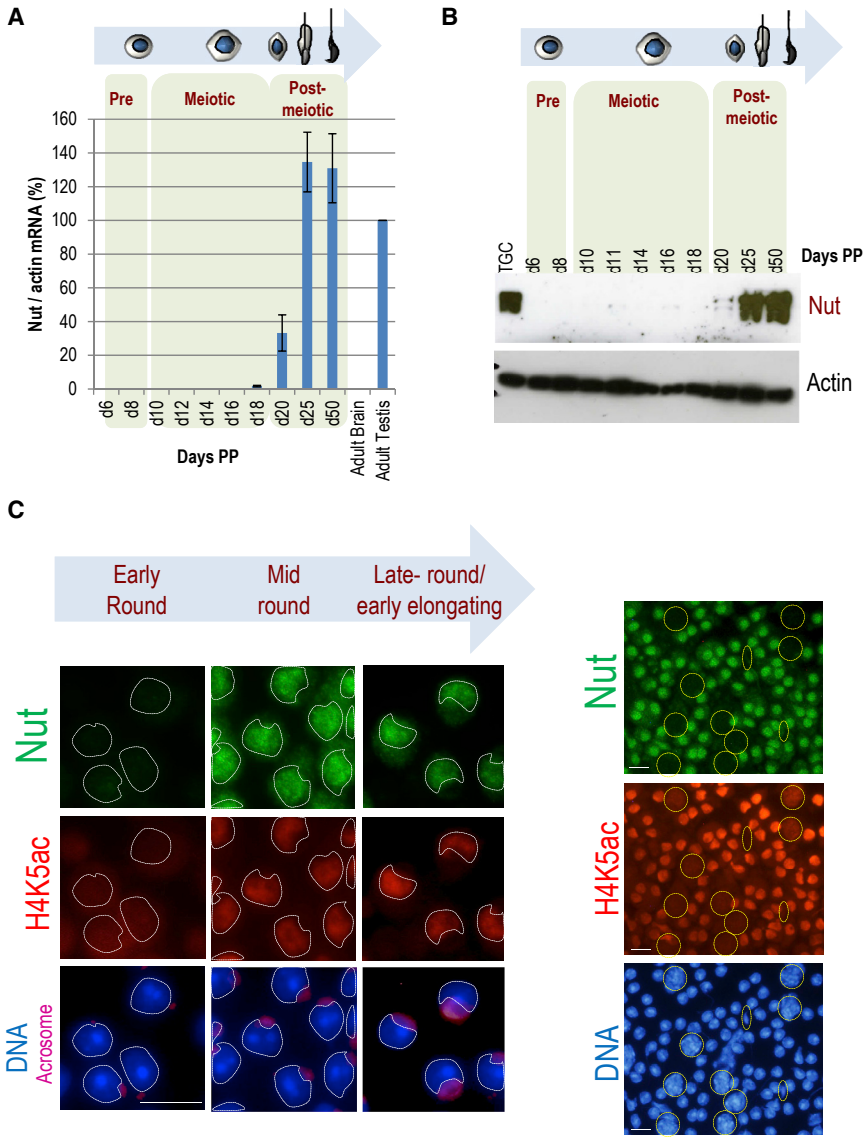

Figure 1. Nut Is Exclusively Expressed in Post-meiotic Spermatogenic Cells and Is Associated with Enhanced Histone H4 Hyperacetylation

(A) RNA was prepared from testes harvested at the indicated times after birth, and the expression of *Nut* was monitored by qRT-PCR, normalized with respect to *actin* expression and represented as the percentage of *Nut* expression in adult testis. Adult testis and adult brain RNAs were used as positive and negative controls, respectively. The histograms represent four experiments. Values represent averages ± SDs (error bars).

(B) In another set of experiments, protein extracts were prepared from testes harvested as described in (A). The corresponding immunoblot was successively probed with the anti-Nut and anti-actin antibodies.

(C) In the left panels, cells from seminiferous tubule preparations were used to co-detect in the same cells Nut (rabbit polyclonal antibodies) and H4K5ac (mouse monoclonal antibody). Lectin was used to simultaneously visualize the acrosomes (in pink). The right panels show images of Nut-expressing round spermatids mixed with spermatocytes and a few condensed spermatids (indicated) taken at lower magnification. The staining was performed as for left panels, except that lectin was not used.

Scale bars: 10 μm. See Figure S1 for tissue-specific patterns of *Nut*/*NUT* expression in human and mouse tissues.

oncogenic activity of the fusion protein BRD4-NUT revealed that it mediates the creation of hyperacetylated chromatin domains. In cells expressing BRD4-NUT, a feed-forward loop drives histone acetylation propagation (Reynoird et al., 2010). This BRD4-NUT-driven histone acetylation is constrained by cellular deacetylases (Reynoird et al., 2010; Schwartz et al., 2011) and remains limited to the nuclear topologically associated domains (TADs) (Alekseyenko et al., 2015), leading to the creation of hyperacetylated chromatin domains.

The discovery of the molecular basis of the activity of the fusion protein BRD4-NUT in NMC and of a role for NUT in inducing enhanced histone acetylation in NMC cancer cells prompted us to propose that Nut could also have a role in inducing the genome-wide histone hyperacetylation in post-meiotic male germ cells. To explore this hypothesis, we designed a series of experiments aiming to address the role of Nut during spermatogenesis at a molecular level.

The investigations reported here reveal mechanisms underlying the obscure process of histone H4 hyperacetylation and its molecular link to the genome-wide histone eviction. These data also demonstrate that the functional cooperation of Nut, p300 and/or CBP, and a BET factor that is created following the *BRD4-NUT* gene fusion in NMC also exists in the natural setting of Nut's action, the post-meiotic spermatogenic cells. The sequence of events triggered by this interaction becomes oncogenic when it operates "off context."

RESULTS

Nut Is a Testis-Specific Factor Exclusively Expressed in Post-Meiotic Spermatogenic Cells

The fusion partner of *BRD4*, *NUT*, was identified as a gene expressed in testis. However, until now, no information was available on its tissue-specific activity or on the pattern of its expression in testis during male germ cell differentiation.

Using publicly available transcriptomic data from different human and mouse tissues, we found that in both human and mouse, *NUT*/*Nut* is exclusively expressed in testis (Figure S1). We prepared RNA and protein extracts from developing mouse testes to precisely define the timing of

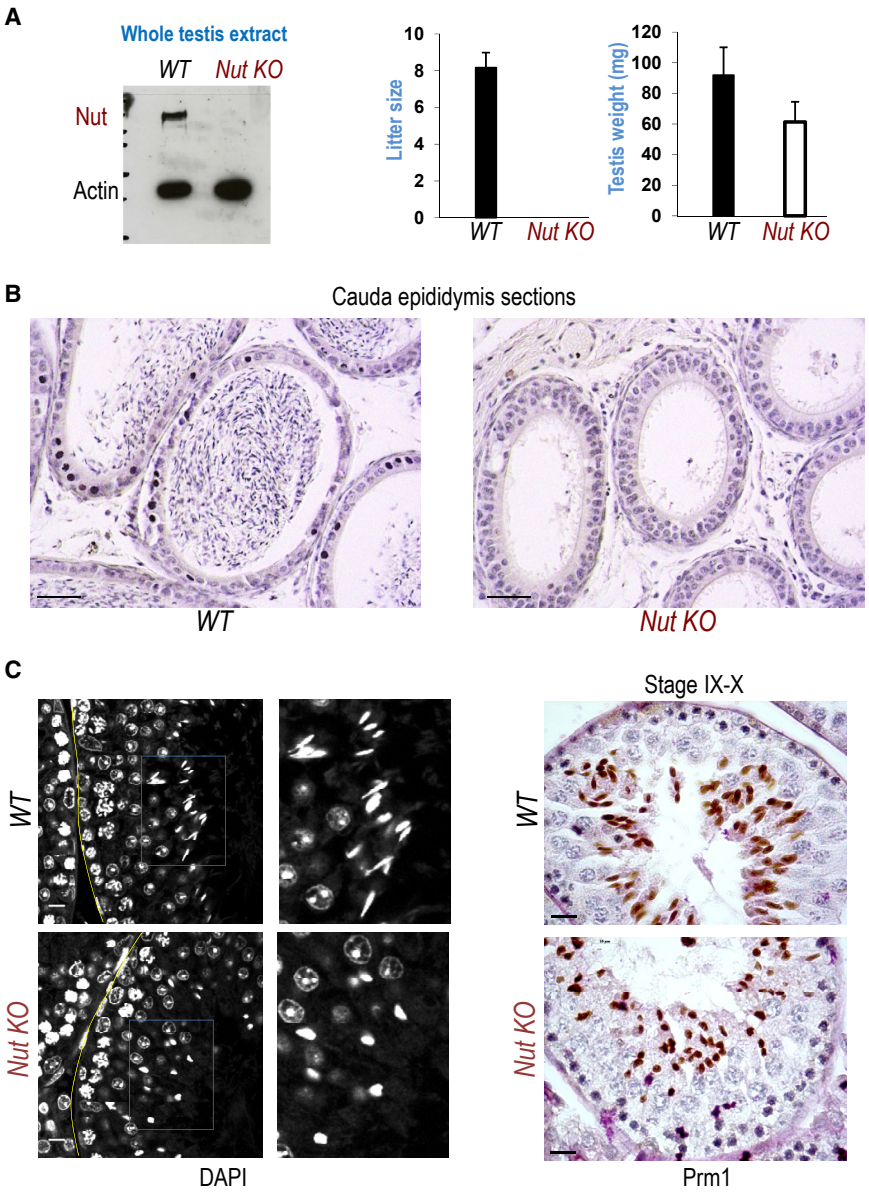

Figure 2. Inactivation of the *Nut* Gene Leads to Spermatogenesis Arrest and Male Infertility

(A) Protein extracts from wild-type and *Nut KO* mouse testes were probed with the anti-Nut and anti-actin antibodies as indicated (left panel). The right panels show litter sizes obtained after crossing wild-type female mice with wild-type (n = 12) or *Nut KO* (n = 5) male mice. The average weights of testes of wild-type (n = 16) and *Nut KO* (n = 19) mice were determined. Litter sizes and testis weights are represented as histograms. Each histogram represents averaged values ± SDs (error bars).

(B) Histological preparations of cauda epididymis from wild-type or *Nut KO* mice are shown as indicated. Scale bar: 50 μm.

(C) Histological sections of paraffin-embedded testes from wild-type and *Nut KO* mice testes at stages IX and X of spermatogenesis were stained with DAPI (left panels). The regions corresponding to the insets are shown at a higher magnification on the right. The right panels show the same types of sections as in the left panels but immunostained with an anti-Prm1 antibody and counterstained with hematoxylin. Scale bars: 10 μm.

See Figure S2 for the *Nut KO* strategy.

Nut gene expression and Nut protein accumulation during spermatogenesis.

Post-meiotic haploid round spermatids first appear at 20 days post-partum (dpp). Traces of *Nut* mRNA (Figure 1A) and protein (Figure 1B) also appear at day 20. Both *Nut* mRNA and protein strongly accumulate at 25 dpp, when late round and early elongating spermatids are produced. *In situ* co-detection of Nut, along with the acrosome on spermatogenic cell preparations, shows that Nut is not detectable in early round spermatids, as defined by the size of their acrosomes, but instead accumulates in mid-round, late round, and early elongating spermatid populations (Figure 1C, left panel).

The observed timing of Nut accumulation in round and early elongating spermatids corresponds to when histone H4 hyperacetylation is known to first occur (Goudarzi et al., 2014). This observation prompted us to co-detect Nut and H4K5ac (acetyl), a critical histone mark in post-meiotic cells (Gaucher et al., 2012; Goudarzi et al., 2016). Figure 1C (left panels) shows that the accumulation of Nut is associated with the induction of histone H4K5 acetylation in differentiating spermatids. Additional *in situ* co-detection of Nut and H4K5ac confirms this strict correlation between the accumulation of Nut and the occurrence of enhanced H4K5 acetylation. Only background H4K5ac could be detected in spermatocytes that do not express Nut compared to Nut-expressing round spermatids (Figure 1C, right panel).

The question therefore arose of whether Nut could be a direct player in the induced acetylation of histone H4 in early elongating spermatids.

Nut Is Essential for the Completion of Spermiogenesis and Mature Sperm Production

To evaluate the function of Nut in post-meiotic spermatogenic cells, we set up a strategy based on the deletion of *Nut* exon 2 to generate $Nut^{KO/KO}$ mice (*Nut* knockout [*Nut KO*] mice) (Figure S2). Western blots using our antibody on total testis extracts demonstrated the absence of Nut in spermatogenic cells of *Nut KO* mice (Figure 2A, left panel). *Nut KO* mice harbored smaller testes and were sterile (Figure 2A, middle and right panels). Cauda epididymis from *Nut KO* mice showed the absence of spermatozoa (Figure 2B), demonstrating an arrest

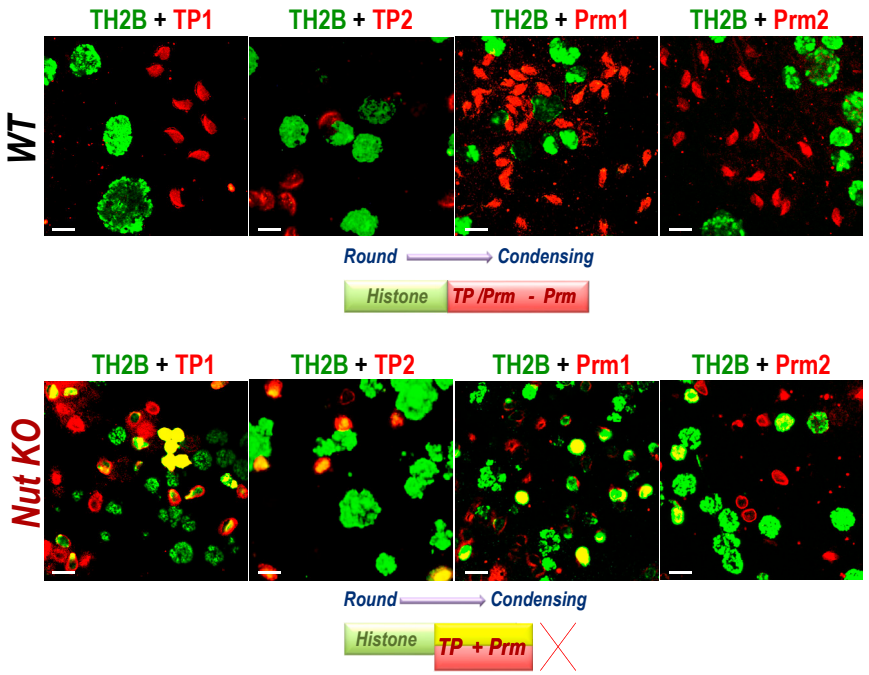

Figure 3. Nut Is Required for Histone-to-Protamine Replacement

TH2B (in green) was co-detected, along with TP1, TP2, Prm1, and Prm2 (in red) in wild-type and *Nut KO* male germ cells. See also Figure S3, showing Prm1 detection in both *Nut KO* and *Brdt ΔBD1/ΔBD1* elongating and condensing spermatids. Scale bars: 10 μm.

of spermatogenesis at earlier stages. To precisely define spermatogenesis stages affected by the absence of Nut, we prepared histological sections of paraffin-embedded testes from wild-type (*WT*) and *Nut KO* mice. In *Nut KO* mice testes, spermatogenesis seems to occur normally until the appearance of condensing spermatids. Although round spermatids could be easily detected in both wild-type and *Nut KO* testes, no condensing spermatids were found in *Nut KO* testes (Figure 2C, DAPI panels). Immunohistochemistry on these sections using an anti-Prm1 antibody showed that in the absence of Nut, the Prm1-expressing spermatids do not undergo nuclear elongation and mostly remain round (Figure 2C, Prm1 panels).

Because Nut accumulation is associated with the induction of histone H4 acetylation (Figure 1C), which is associated with the replacement of histones by TPs and protamines (Gaucher et al., 2012; Goudarzi et al., 2016), we focused on the process of histone-to-protamine replacement. Accordingly, TH2B, which is the major spermatogenic cell histone H2B variant (Montellier et al., 2013), was co-detected, along with histone-replacing proteins TP1, TP2, Prm1, and Prm2. Figure 3 shows that although TH2B was never observed in wild-type cells expressing histone-replacing proteins, in *Nut KO* spermatids, TH2B was co-detected with TP1, TP2, Prm1, and Prm2. These observations demonstrate that even though the histone-replacing proteins are expressed in the absence of Nut, they are incapable of replacing histones.

To further demonstrate the defective histone replacement in the *Nut KO* spermatids, we made the hypothesis that the accumulation of TPs and protamines in the absence of histone replacement should leave an imprint on nucleosomes, especially on the more accessible DNA linker regions. The interaction of these highly basic proteins with linker DNA should protect DNA linker regions against micrococcal nuclease (MNase) digestion and therefore generate DNA fragments longer than the canonical 147 base pairs (bp). To test this hypothesis, we prepared nuclei from fractionated round-elongating spermatids from wild-type and *Nut KO* testes and submitted them to extensive digestion with MNase to generate nucleosomal monomers. We then used paired-end sequencing to accurately determine DNA fragment lengths at the highest (base pair) resolution following two independent experiments (different mice and different fractionations). Both experiments revealed an enrichement of nucleosomal DNA fragments with lengths longer than the canonical 147 bp in *Nut KO* spermatids compared to wild-type spermatids (Figures 4A and 4B).

Altogether, the co-immunodetection of TH2B and histone-replacing proteins, as well as the accumulation of nucleosomes with longer linker DNA in *Nut KO* spermatids, strongly support an impairment of histone replacement in the absence of Nut.

The defective histone replacement observed in the absence of Nut was reminiscent of the impaired TP and protamine assembly previously detected in mouse spermatogenic cells expressing a Brdt mutant lacking its first bromodomain (BD1) (Gaucher et al., 2012) (Figure S3), suggesting a possible functional link between Nut and Brdt's first bromodomain in histone replacement.

Nut Sustains Site-Specific Histone Acetylation

Because Brdt's BD1 binds to histone H4 acetylated on K5 and K8 (Goudarzi et al., 2016; Miller et al., 2016; Morinière et al., 2009; Sasaki et al., 2009), and Brdt's BD1 is necessary for histone-to-protamine replacement (Gaucher et al., 2012), the impairment of histone removal in the absence of Nut (Figures 3 and S3) could be attributed to the absence of functional Brdt or to a defective histone acetylation specifically at H4K5 and H4K8.

A western blot on extracts from fractionated post-meiotic round and early elongating spermatids showed no change in the level of Brdt expression in the absence of Nut (Figure 5A). This result, along with our observation that Nut accumulation in mid- and late round and early elongating spermatids corresponds to the induction of histone hyperacetylation (Figure 1C), prompted us to perform a comparative analysis of the level of histone acetylation on histones extracted from round and early elongating spermatids from wild-type and *Nut KO* testes.

Consequently, we sought an unbiased approach to quantitatively monitor histone acetylation in the wild-type and *Nut KO*

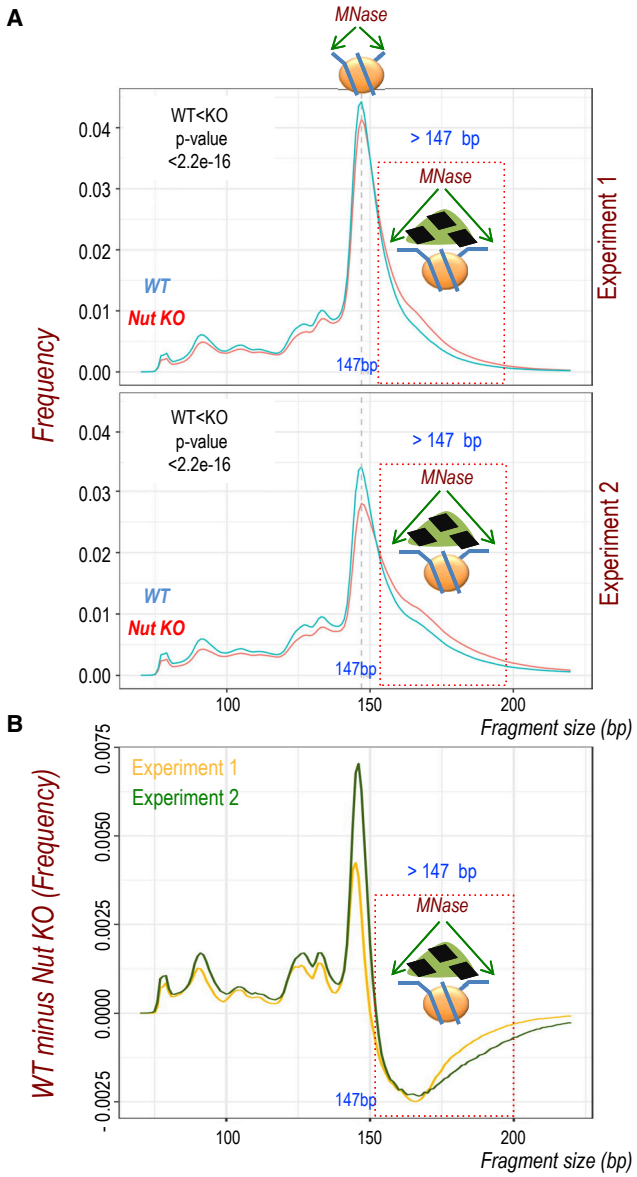

Figure 4. Genome-wide High-Resolution Studies Show Chromatin Changes in *Nut KO* Spermatids

(A) Paired-end sequencing was used for the high-resolution determination of nucleosomal DNA fragment lengths protected against extensive MNase digestion of nuclei prepared from fractionated spermatids from *wild-type* and *Nut KO* testes. Standard MNase fragment size distributions (mode at 147 bp) are observed for the two independent experiments. A more prominent shift toward DNA lengths > 147 bp is observed in *Nut KO* spermatids. The length shift significance was statistically assessed using a one-sided Wilcoxon rank-sum test with continuity correction.

(B) Comparison by subtraction of *wild-type* versus *Nut KO* distribution frequency of fragment size, highlighting the enrichment of standard nucleosomes and sub-nucleosomal structures in *wild-type* spermatids and the enrichment of longer nucleosomal DNAs in the chromatin of *Nut KO* spermatids. The results of two independent experiments are shown. For each experiment, round spermatid fractions were obtained from 3 to 5 mice (6 to 10 testes) and nuclei were prepared and extensively digested by MNase to reduce chromatin to nucleosome monomers. The nucleosomal DNA obtained from each experiment was then purified and used for paired-end sequencing.

round and early elongating spermatids. *In vitro* isotopic labeling followed by high-performance liquid chromatography-tandem mass spectrometry (HPLC-MS/MS) analysis was performed to quantify histone post-translational modifications (PTMs). Histone extracts were digested with trypsin, and the resulting peptides were propionylated using light ($^{12}C_6$) and heavy ($^{13}C_6$) propionic anhydride. The light and heavy propionylated tryptic peptides were mixed in equal amounts and analyzed by HPLC-MS/MS.

The quantification of histone acetylation revealed a decrease in histone H4 and H2A acetylation, with a remarkable downregulation of acetylation at H4K5 and H4K8, as well as of H2AK5 and H2AK9 (Figure 5A, lower panel; Tables S1 and S2).

The downregulation of acetylation, especially at the critical H4K5 and H4K8 sites, in *Nut KO* round and early elongating spermatids compared to the wild-type spermatids was confirmed by western blotting, with the corresponding antibodies on independently prepared round and early elongating spermatid-enriched fractions (Figure 5B). Because none of the H3 tail lysines analyzed here by mass spectrometry were significantly affected by the absence of Nut, H3K9 acetylation was additionally checked by immunoblotting, showing only a slight decrease in *Nut KO* spermatids (Figure 5B).

These results show that the expression of *Nut* in round and early elongating spermatids (Figure 1C) is required for histone H4 hyperacetylation. In addition, the impairment of Nut-mediated acetylation of H4 demonstrates the inability of Brdt's BD1 to bind chromatin, explaining the similarity between *Nut KO* and $Brdt^{delta\ BD1/delta\ BD1}$ phenotypes (Figure S3).

Nut Controls the Expression of a Subset of Genes Expressed in Spermatids

Our previous work on NMC identified p300 and/or CBP as the major cellular histone acetyltransferases (HATs) recruited by the NUT moiety of the BRD4-NUT fusion protein in a NMC cell line or upon transfection (Reynoird et al., 2010). We therefore hypothesized that when expressed in its physiological setting, spermatids, Nut could interact with p300 and/or CBP and use a similar mechanism to enhance histone acetylation. To verify this hypothesis, we performed two independent sets of experiments. First, the round and early elongating spermatid fractions from wild-type and *Nut KO* testes were used to obtain and compare the corresponding transcriptomes and to identify genes whose expression depends on Nut. The absence of Nut was found to be associated with the downregulation of 1,184 genes and the upregulation of 499 genes (using a cutoff of 1.5 for the absolute log2 fold change value and a t test p value, after adjustment for multiple tests by Benjamini-Hochberg, of $p < 0.05$) (Figure 6A).

To ensure the observed changes in gene expression in the absence of Nut were not due to changes in the cell-type composition of the *Nut KO* round and elongating cell fraction compared to the same fraction of wild-type cells, we performed an additional analysis. By comparing wild-type meiotic and post-meiotic cell populations, we identified genes that are normally activated in wild-type post-meiotic cells. The observation that only a fraction of these genes was downregulated in *Nut KO* post-meiotic cells was supportive of a specific action of Nut on gene

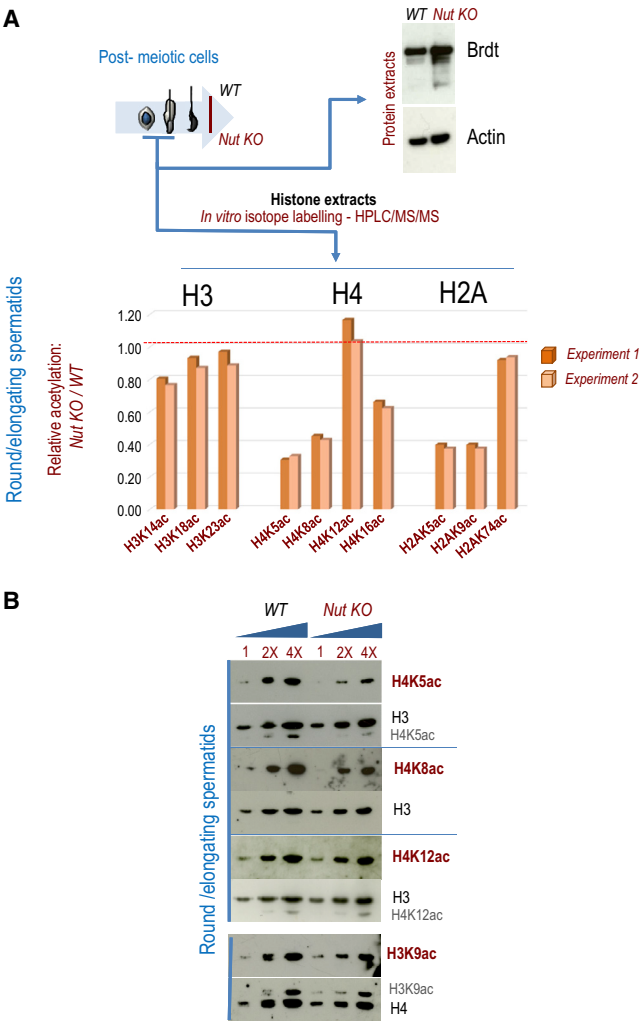

Figure 5. Nut Sustains Histone H4 Hyperacetylation in Spermatids

(A) Spermatogenic cell suspensions from wild-type and *Nut KO* testes were fractionated to prepare cell suspensions enriched in round and elongating spermatids. In one experiment, the corresponding extracts were used to detect Brdt and actin as indicated. In another experiment, histone extracts from these fractions (wild-type and *Nut KO*) were analyzed by *in vitro* isotopic labeling followed by HPLC-MS/MS. The relative abundance of identified site-specific acetylation was determined and expressed as the ratio *Nut KO*/wild-type. H3, H4, H2B, and H2A peptides were used to normalize the *Nut KO*/wild-type samples. For more information on the normalization process, refer to Table S2 and its legend and to Quantification of Histone PTMs.

(B) Independent cell fractionation experiments were set up to prepare extracts from round and elongating spermatid-enriched fractions. Increasing amounts of extracts (1×, 2×, and 4×) were used for immunoblots as indicated. H4K5ac, H4K8ac, and H4K12ac were visualized with the corresponding specific antibodies in wild-type and *Nut KO* cell extracts as indicated. Each of these blots was re-probed with anti-H3 antibody as indicated. H3K9ac was also detected (lowest panel) and the corresponding blot was re-probed with anti-H4 antibody (the remaining H4K5ac, H4K12ac, and H3K9ac signals after anti-H3 and anti-H4 re-probing are indicated in gray letters).

expression as opposed to the loss of particular cell types. The expression of a significant number of the genes, 317, including the Prm1-encoding gene, that are normally activated in wild-type post-meiotic cells did not significantly change in the absence of Nut (Figures S4A and S4B), demonstrating that our transcriptomic data from wild-type and *Nut KO* spermatids could be compared, because they were obtained from two comparable cell populations.

We then used a series of stage-specific transcriptomes that were produced in wild-type male germ cells from our previous studies (Boussouar et al., 2014; Montellier et al., 2013) and the present work to establish the normal pattern of these Nut-regulated genes during spermatogenesis. Figure S4C shows that the genes that require Nut to be active (downregulated genes in *Nut KO*) are normally activated in post-meiotic cells, with the highest activity in late round and early elongating spermatids.

In a previous work, we identified genes that are specifically responsive to post-meiotic p300 and/or CBP variations in spermatids (Boussouar et al., 2014). We used these data to define whether Nut regulates gene expression through p300 and/or CBP by comparing our two Nut- and p300 and/or CBP-dependent transcriptomes, both obtained in comparable post-meiotic cell populations. We looked for a significant enrichment of Nut-regulated genes in the lists of p300 and/or CBP-regulated genes, which would suggest the involvement of p300 and/or CBP in gene regulation by Nut. Gene set enrichment analysis (GSEA) was used to look for the expression in *Nut KO* spermatids of genes whose expression in spermatids had previously been found to be affected by a targeted post-meiotic deletion of *p300* and *CBP* (Boussouar et al., 2014). Although following this latter approach, the inheritance of both p300 and CBP from preceding stages led to only a small decrease in the enzyme levels in post-meiotic cells, it was enough to observe a change in the expression of a specific set of genes whose expression is highly dependent on, and sensitive to, p300 and CBP dosage (Boussouar et al., 2014).

Figure 6B shows a clear enrichment of the p300 and/or CBP-regulated genes among the genes up- and downregulated in *Nut KO* mice, supporting the idea that Nut-p300 and/or CBP, while directing the global histone acetylation, also affects the expression of late active genes before the general shutdown of transcription in elongating spermatids.

p300 and/or CBP Are the Only Acetyltransferases Present in the Nut Interactome

The question arises of whether Nut uses CBP and p300 in spermatids as it does in NMC cells or if other HATs are also involved. To answer this question, in an additional set of experiments, we prepared extracts from fractionated wild-type and *Nut KO* round and early elongating spermatids, which were submitted to anti-Nut immunoprecipitation and a proteomic analysis in two independent assays.

The aim of this experiment was two-fold: first, to confirm the presence of p300 and CBP in association with Nut, and second, to see whether additional cellular acetyltransferases interact with Nut in post-meiotic cells undergoing histone hyperacetylation. To maximize the chance of detecting any HAT associated with Nut, we used non-stringent immunoprecipitation conditions and performed the experiment twice on independent mice and fractionated cells. As expected from non-stringent immunoprecipitation conditions, many proteins were identified as

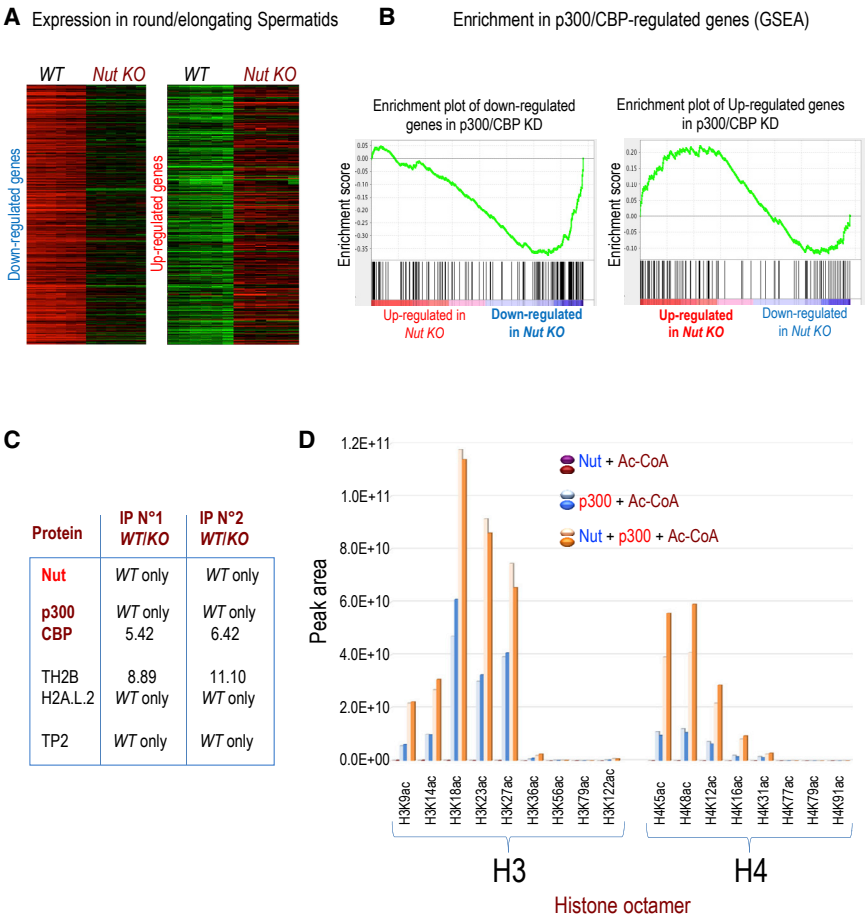

Protein	IP N°1 WT/KO	IP N°2 WT/KO
Nut	*WT* only	*WT* only
p300	*WT* only	*WT* only
CBP	5.42	6.42
TH2B	8.89	11.10
H2A.L.2	*WT* only	*WT* only
TP2	*WT* only	*WT* only

Figure 6. Nut Is Involved in the Control of Gene Expression by p300 and/or CBP and Uses p300 to Acetylate Histones

(A) Round and elongating spermatid fractions were obtained as in Figures 5A and 5B, but this time RNA was purified and used to compare the transcriptomes of *Nut KO* cells and wild-type cells. The heatmaps show genes that are down-regulated (left panel, n = 1,184) and upregulated (right panel, n = 499) in *Nut KO* compared to wild-type round and elongating spermatids. See Figure S4 and its legend.

(B) Gene set enrichment analysis (GSEA) (http://software.broadinstitute.org/gsea/) in the *Nut KO* versus wild-type transcriptomic experiment (obtained in A) was performed for two lists of genes (used as gene sets) previously established as downregulated or upregulated in round and elongating spermatids after the conditional post-meiotic knockout of *p300* and *CBP* (Boussouar et al., 2014). Genes that are down- or upregulated after double *p300* and/or *CBP KO* are significantly enriched in genes that are, respectively, down- or upregulated in *Nut KO* spermatids.

(C) Spermatogenic cell fractions identical to those shown in (A) and Figure 5 were used to perform the immunoprecipitation of Nut. Mass spectrometry was then used to identify Nut-associated proteins, meaning proteins present or significantly enriched in the wild-type cell extracts and absent from *Nut KO* cell extracts. The wild-type/*KO* ratio of proteins corresponding to the only identified HATs (p300 and CBP), as well as proteins known to be involved in histone-to-protamine replacement, is shown. The indicated values represent protein enrichment in wild-type cell immunoprecipitations over *Nut KO*. The list of identified proteins functionally linked to chromatin and/or transcription and/or RNA and/or metabolism is presented in Table S3.

(D) Reconstituted histone octamers were incubated with acetyl-CoA, as well as purified p300 (residues 340–2,094: $p300_{short}$) and the p300-interacting domain of NUT as indicated. HPLC-MS/MS was used to quantify site-specific H3 and H4 acetylation by label-free quantification *in vitro*. Five high-abundance unmodified peptides were used to normalize the amount of each histone. The peak area of histone octamer was then normalized, and the data corresponding to two experiments are shown (with different color codes as indicated). See related Figure S5.

specifically enriched in *Nut* wild-type cells and were observed in both experiments. However, in an effort to focus on proteins relevant to the present study, especially HATs, we chose to highlight the transcription and/or chromatin and/or RNA and/or metabolism-related proteins. Table S3 lists the proteins that were only found in the wild-type cell extracts or enriched at least 5 times in these extracts compared to *Nut KO* cell extracts. Despite the non-stringent immunoprecipitation conditions, p300 and CBP were the only known HATs found to be exclusively or significantly enriched in the Nut immunoprecipitates in wild-type extracts compared to *Nut KO* extracts (Figure 6C). In the Nut-dependent proteome, we also found TH2B-H2A.L.2 and transition protein 2 (TP2), shown to allow protamines to efficiently invade nucleosomes at the time of histone-to-protamine replacement (Barral et al., 2017) (Figure 6C). Because the generation of these nucleosomal transitional states also involves H4 acetylation and Brdt's BD1, these findings reinforce the hypothesis that Nut could also be a player in the process of acetylation-dependent histone replacement.

A proteomic analysis of BRD4-NUT fusion partners from a human cell line generated similar data, with p300 and CBP as the only BRD4-NUT-associated HATs (Alekseyenko et al., 2017), confirming our early finding that p300 and CBP are the major HAT partners of NUT (Reynoird et al., 2010). Altogether, these data are in agreement with our comparative transcriptomic analysis (Figure 6B), pointing to p300 and/or CBP as the only cellular HAT partners of Nut.

Nut Enhances p300-Induced H3 and H4 Acetylation

We previously demonstrated that p300 interacts with a specific fragment of NUT, which stimulates its HAT activity on purified histone H3 (Reynoird et al., 2010). Here, to have a comprehensive vision of the action of Nut on histone acetylation, and more specifically to evaluate the action of NUT on site-specific histone acetylation by p300, we incubated purified recombinant p300 with the p300-interacting fragment of NUT and histone octamers (Figure S5). Isotopic labeling following HPLC-MS/MS was used to quantitatively measure the impact of NUT on

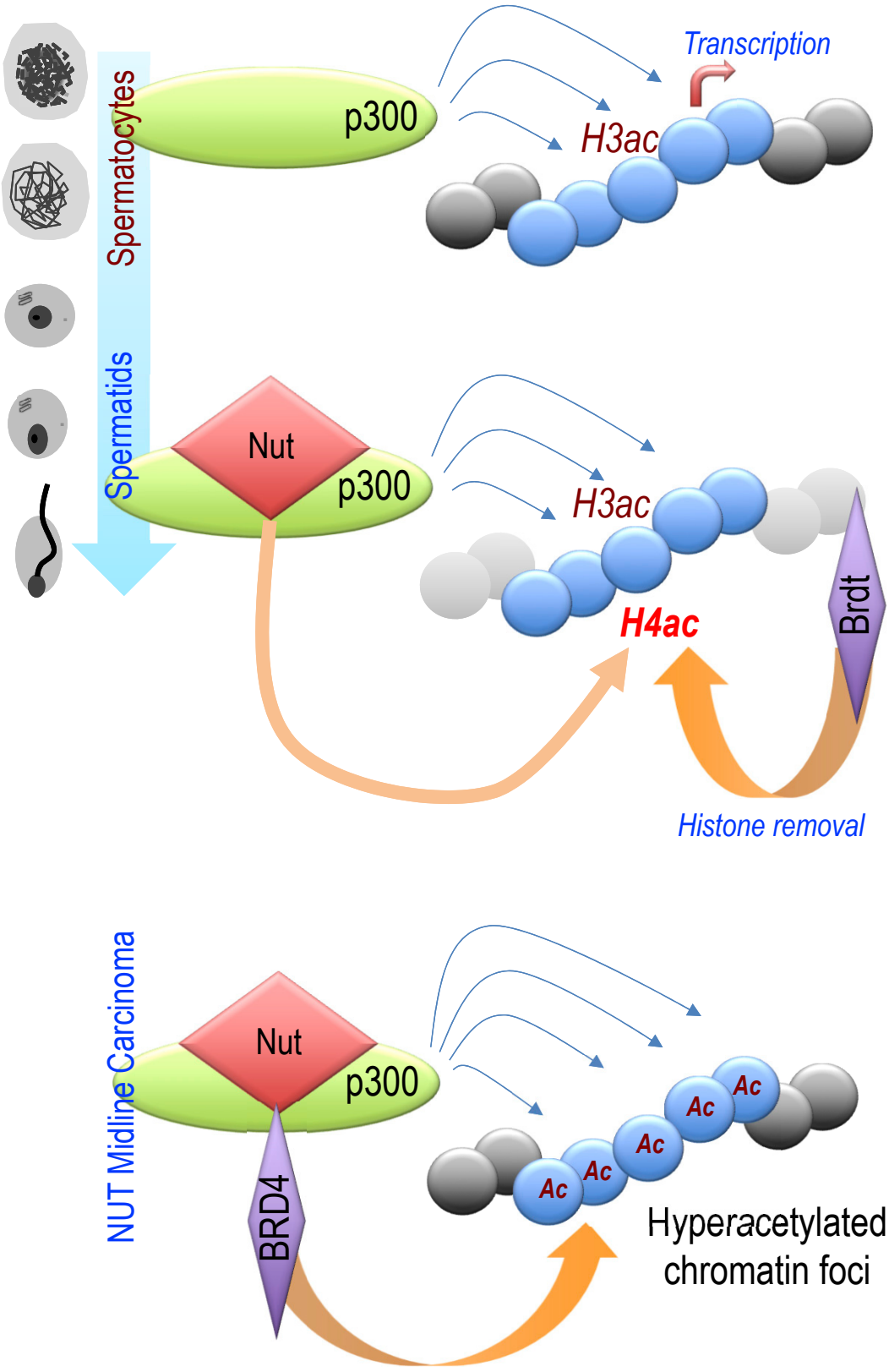

(legend on next page)

p300-mediated histone H3 and H4 acetylation. In histone octamers, p300 more efficiently acetylated histone H3 compared to histone H4 (p300 + Ac-coenzyme A [CoA]) (Figure 6D). For both histones, acetylation occurred at the tails, with no significant acetylation of the internal lysines (Figure 6D). The addition of the p300-interacting fragment of NUT enhanced H3 and H4 tail acetylation (Figure 6D; Tables S4 and S5; Figure S5). These data were confirmed after independent HAT assays following immunodetection with two site-specific antibodies against H3K9ac and H4K5ac (Figures S5B and S5C).

Altogether, these data show that Nut directly recruits p300 and/or CBP to control both histone H3 and H4 acetylation, although *in vivo*, in early elongating spermatids, the most important impact is observed on H4 acetylation. In contrast to the action of Nut on H3 and H4 acetylation observed *in vitro* (Figure 6D), although the absence of Nut affected H4 acetylation in round and elongating spermatids, none of the considered H3 acetyl acceptor sites seemed to be significantly affected by the absence of Nut (Figure 5).

DISCUSSION

Quantitative measurements of Nut-dependent histone acetylation in round and early elongating spermatids reported here demonstrated that Nut has a histone-specific and site-specific action on chromatin acetylation, particularly targeted on H2A and H4, including H4K5 and H4K8 acetylation.

A wave of histone hyperacetylation had long been described in elongating spermatids. In this context, H4 acetylation seems to play a central role, because it provides a specific binding site for the essential factor involved in histone removal, Brdt (Goudarzi et al., 2014, 2016).

All investigations reported here point to p300 and/or CBP as major HATs, which in addition to a role in maintaining a basal acetylation of H3, become involved in H4 hyperacetylation in post-meiotic cells because of the expression of Nut. However, an important question was whether Nut could control the activity of other HATs in post-meiotic spermatogenic cells to direct the observed H4 hyperacetylation. Our Nut interactomic analysis shows that p300 and CBP are the only cellular Nut-interacting HATs. In an immunopurification of BRD4-NUT followed by mass spectrometry identification of the associated proteins, p300 and CBP were the only HATs found in a complex with BRD4-NUT in somatic cells (Alekseyenko et al., 2017), which highlights the conserved mode of action of Nut both in spermatogenic cells and after its ectopic expression in NMC cancer cells.

Although the action of Nut on H4 acetylation seems to be dramatic, its transcriptional regulatory role only concerns a subset of genes expressed in transcriptionally active late spermatids. Our data show that in round and early elongating spermatids, most Nut-regulated genes are those previously found to be highly sensitive to the cellular levels of p300 and CBP in elongating spermatids before the transcriptional shutdown (Boussouar et al., 2014). It is therefore possible that the enhancement of H4 acetylation by Nut-p300 and/or CBP, in addition to the basal role of these HATs in H3 acetylation (Figure 6) in elongating spermatids, in preparation for histone replacement, stimulates a subset of genes that are normally active immediately before the general transcriptional inactivation.

These data therefore depict Nut's function in post-meiotic germ cells. Nut appears as a stimulator of p300 and CBP, which, in addition to H3 acetylation that normally occurs in spermatogonia and spermatocytes, drives cell-type-specific H4 hyperacetylation in post-meiotic cells in preparation for histone eviction. This gene is exclusively expressed in cells in which global H4 hyperacetylation naturally occurs, strongly supporting this conclusion. In agreement with a role of histone hyperacetylation in histone removal and a role of Nut in H4 hyperacetylation, we observed that in the absence of Nut, the acetylation of histone H4 is downregulated and histone removal is impaired.

The similarity of phenotypes between *Nut* KO and $Brdt^{deltaBD1/deltaBD1}$ mouse models also supports a role of Nut in histone acetylation that occurs upstream of histone removal. In both cases, although TPs and protamines are produced, they are unable to replace histones. This observation strongly suggests that Nut and Brdt function in the same molecular pathway, leading to histone-to-protamine replacement. The molecular mechanism linking Nut activity to histone acetylation, specifically that of H4K5 and H4K8, explains how Nut and Brdt are functionally related. In *Nut KO*-elongating spermatids, because of insufficient acetylation of H4, Brdt's BD1 remains non-functional, leading to the same phenotype as observed in $Brdt^{deltaBD1/deltaBD1}$ cells.

These studies also place Nut at the heart of the molecular mechanisms controlling histone-to-protamine replacement. Nut could link histone hyperacetylation to histone exchange and nucleosome invasion by protamines (Barral et al., 2017). Our Nut-interactomic approach also identified TH2B, H2A.L.2, and TP2 as Nut partners. Therefore, p300 could be part of a machinery that would couple histone H4 acetylation, Brdt binding, and the exchange of TH2B-H2A for TH2B-H2A.L.2 in a series of events that are essential for nucleosome opening and TP-controlled protamine invasion of nucleosomes and histone replacement (Barral et al., 2017). In agreement with this hypothesis, published data have reported the ability of p300 to cooperate with Nap1 to mediate nucleosome disassembly (Asahara et al., 2002; Luebben et al., 2010; Sharma and Nyborg, 2008).

Therefore, at the time of p300-Nut interaction and histone H4 hyperacetylation, nucleosomes adopt an increasingly open configuration and are largely remodeled. It is possible that under these conditions, histone accessibility to HATs such as p300 becomes similar to that of histones in octamers rather than histones

Figure 7. Model for the Cooperation between Nut-p300 and/or CBP-BET in Physiological and Pathological Settings

Along spermatogenesis, the ubiquitous HATs p300 and/or CBP drive transcription, mainly through histone H3 acetylation. Upon its expression in late round and elongating spermatids, Nut interacts with p300 and/or CBP and stimulates its HAT activity, leading to a genome-wide increase in H4 acetylation, specifically at H4K5 and H4K8. Brdt uses its first bromodomain to recognize the two indicated sites on H4 to bind chromatin and to eventually replace histones (upper panel). In NMC cells, where a chromosomal translocation fuses *BRD4* to *NUT*, p300 recruitment by the fusion protein creates an obligatory functional loop involving cycles of NUT-stimulated histone acetylation and BRD4-NUT binding (lower panel).

in regular nucleosomes. In our *in vitro* HAT assays, histone octamers were used instead of nucleosomes. In our hands, nucleosomes seemed to be poor substrates for p300. However, in spermatids *in vivo*, in contrast to our *in vitro* conditions, Nut seems to be indispensable for H4 acetylation, whereas its absence seems to have only minor effects on H3 acetylation. It is possible that *in vivo*, in spermatids, H3 acetylation is inherited from earlier stages and that only H4 acetylation occurs *de novo* at the time of Nut synthesis. This hypothesis is in good agreement with our previous observations that in post-meiotic cells, CBP and p300 are mostly inherited from earlier stages (Boussouar et al., 2014). This possibility could therefore explain why *in vivo* Nut only affects H4 acetylation, which occurs *de novo* in these cells, while most H3 acetylation comes from the preceding stages (Figure 7).

Hence, our data support the hypothesis that Nut is a factor required by CBP and p300 to include H4 as a substrate *in vivo* and ensure H4 hyperacetylation in spermatids. In contrast, its impact on the level of H3 acetylation *in vivo* is relatively modest, because these enzymes already efficiently acetylate H3 in male germ cells at earlier stages of spermatogenesis (Figure 7).

In summary, we found that Nut's major function is to direct histone H4 hyperacetylation, leading to the cooperative action of p300, CBP, and the BET factor Brdt in haploid male germ cells. In NMC cells, a chromosomal translocation induces NUT-mediated forced cooperation between p300 and/or CBP and BRD4 to induce hyperacetylated histone chromatin foci (Figure 7). An extension of this work would be to explore the similarities between NMC cells and elongating spermatids. Rescue experiments with *Nut* re-expression under the control of different promoters, active at earlier stages of spermatogenesis, could be performed in the context of mice bearing *Nut KO* alone or both *Nut KO* and *Brdt*$^{deltaBD1/deltaBD1}$, which would demonstrate the cooperation between Nut and BD1 in the process of histone hyperacetylation.

This work also highlights a concept that cells can use particular auxiliary factors in a tissue- and cell-type-specific manner to enhance the activity of chromatin-modifying enzymes that are ubiquitously expressed and thus achieve a large-scale, tissue-specific chromatin modification such as H4 hyperacetylation in post-meiotic spermatogenic cells. The ectopic activation of such factors could initiate an oncogenic molecular circuit as it does in NMC cells expressing the BRD4-NUT fusion protein.

STAR★METHODS

Detailed methods are provided in the online version of this paper and include the following:

SUPPLEMENTAL INFORMATION

Supplemental Information includes five figures and five tables and can be found with this article online at https://doi.org/10.1016/j.celrep.2018.08.069.

ACKNOWLEDGMENTS

The S.K. laboratory is supported by a grant from the Foundation pour la Recherche Medicale (FRM), "analyse bio-informatique pour la recherche en biologie" program, as well as by the ANR Episperm3 program and by INCa libre program (RPT13001CCA). Additional support came from the Université Grenoble Alpes (ANR-15-IDEX-02) LIFE and SYMER programs, as well as from Fondation ARC "Canc'air" project (RAC16042CLA) and Plan Cancer (CH7-INS15B66 and ASC16012CSA). Z.I. and D.P. were supported by a Worldwide Cancer Research foundation grant (16-0280) to D.P. H.S. was a recipient of a Marie Curie Initial Training Network funded by European Commission (FP7-PEOPLE-2011-ITN and PITN-GA-289880) for 3 years and then supported by La Ligue Nationale Contre Le Cancer for a 4th year of PhD pursuit. G.C. is a bioinformatic expert benefiting from a FRM fellowship. Mice were bred in the High Technology Animal Facility (PHTA) of Grenoble University with the help of Natacha Pitoun and Kevin Escot. The TGML Platform is supported by grants from Inserm, GIS IBiSA, and Aix-Marseille Université (ANR-10-INBS-0009-10). We are grateful to Hortense Vachon for her help with library preparation and sequencing. The proteomic analyses were partially supported by the French National Research Agency ProFi grant (ANR-10-INBS-08-01). P.F. and S.P. were supported by a Wellcome Trust Cancer Development Fellowship (095751/Z/11/Z). Y.C. thanks the support of the discovery platform and informatics group at EDyP. Most computations presented in this paper were performed using the GRICAD infrastructure (https://gricad.univ-grenoble-alpes.fr).

AUTHOR CONTRIBUTIONS

H.S., S.B., and T.B. performed most experiments. M.T., M.Z., and Y.Z. performed quantitative measurements of *in vivo* and *in vitro* histone acetylation. F.B., T.B., and N.R. designed the *Nut KO* strategy and prepared the necessary materials and controlled the various steps toward mouse production, which was carried out in the M.G. laboratory. Y.C. performed the characterization of the Nut interactome. A.G., Z.I., and D. Panne performed recombinant p300 purification and *in vitro* HAT assays. S.P. and P.F. did Nut fragment purification for anti-Nut antibody production. L.B. constructed and sequenced the library for micrococcal nuclease sequencing (MNase-seq) experiments. G.C., D. Puthier, F.C., E.B.-F., and S.R. performed the bioinformatics analyses. S.K. conceived and coordinated the project and wrote the manuscript. All authors discussed the data and read and commented on the manuscript.

DECLARATION OF INTERESTS

Y.Z. is a shareholder and a member of the scientific advisory board of PTM BioLabs, Co. (Chicago). The other authors declare no competing interests.

Received: April 20, 2018
Revised: July 19, 2018
Accepted: August 23, 2018
Published: September 25, 2018

REFERENCES

Alekseyenko, A.A., Walsh, E.M., Wang, X., Grayson, A.R., Hsi, P.T., Kharchenko, P.V., Kuroda, M.I., and French, C.A. (2015). The oncogenic BRD4-NUT chromatin regulator drives aberrant transcription within large topological domains. Genes Dev. *29*, 1507–1523.

Alekseyenko, A.A., Walsh, E.M., Zee, B.M., Pakozdi, T., Hsi, P., Lemieux, M.E., Dal Cin, P., Ince, T.A., Kharchenko, P.V., Kuroda, M.I., and French, C.A. (2017). Ectopic protein interactions within BRD4-chromatin complexes drive oncogenic megadomain formation in NUT midline carcinoma. Proc. Natl. Acad. Sci. USA *114*, E4184–E4192.

Asahara, H., Tartare-Deckert, S., Nakagawa, T., Ikehara, T., Hirose, F., Hunter, T., Ito, T., and Montminy, M. (2002). Dual roles of p300 in chromatin assembly and transcriptional activation in cooperation with nucleosome assembly protein 1 *in vitro*. Mol. Cell. Biol. *22*, 2974–2983.

Barral, S., Morozumi, Y., Tanaka, H., Montellier, E., Govin, J., de Dieuleveult, M., Charbonnier, G., Couté, Y., Puthier, D., Buchou, T., et al. (2017). Histone variant H2A.L.2 guides transition protein-dependent protamine assembly in male germ cells. Mol. Cell *66*, 89–101.

Boussouar, F., Goudarzi, A., Buchou, T., Shiota, H., Barral, S., Debernardi, A., Guardiola, P., Brindle, P., Martinez, G., Arnoult, C., et al. (2014). A specific CBP/p300-dependent gene expression programme drives the metabolic remodelling in late stages of spermatogenesis. Andrology *2*, 351–359.

Buchou, T., Tan, M., Barral, S., Vitte, A.-L., Rousseaux, S., Arechaga, J., and Khochbin, S. (2017). Purification and analysis of male germ cells from adult mouse testis. Methods Mol. Biol. *1510*, 159–168.

Casabona, M.G., Vandenbrouck, Y., Attree, I., and Couté, Y. (2013). Proteomic characterization of Pseudomonas aeruginosa PAO1 inner membrane. Proteomics *13*, 2419–2423.

Chen, Y., Kwon, S.W., Kim, S.C., and Zhao, Y. (2005). Integrated approach for manual evaluation of peptides identified by searching protein sequence databases with tandem mass spectra. J. Proteome Res. *4*, 998–1005.

French, C.A. (2012). Pathogenesis of NUT midline carcinoma. Annu. Rev. Pathol. *7*, 247–265.

Garcia, B.A., Mollah, S., Ueberheide, B.M., Busby, S.A., Muratore, T.L., Shabanowitz, J., and Hunt, D.F. (2007). Chemical derivatization of histones for facilitated analysis by mass spectrometry. Nat. Protoc. *2*, 933–938.

Gaucher, J., Reynoird, N., Montellier, E., Boussouar, F., Rousseaux, S., and Khochbin, S. (2010). From meiosis to postmeiotic events: the secrets of histone disappearance. FEBS J. *277*, 599–604.

Gaucher, J., Boussouar, F., Montellier, E., Curtet, S., Buchou, T., Bertrand, S., Hery, P., Jounier, S., Depaux, A., Vitte, A.-L., et al. (2012). Bromodomain-dependent stage-specific male genome programming by Brdt. EMBO J. *31*, 3809–3820.

Goudarzi, A., Shiota, H., Rousseaux, S., and Khochbin, S. (2014). Genome-scale acetylation-dependent histone eviction during spermatogenesis. J. Mol. Biol. *426*, 3342–3349.

Goudarzi, A., Zhang, D., Huang, H., Barral, S., Kwon, O.K., Qi, S., Tang, Z., Buchou, T., Vitte, A.-L., He, T., et al. (2016). Dynamic competing histone H4 K5K8 acetylation and butyrylation are hallmarks of highly active gene promoters. Mol. Cell *62*, 169–180.

Liu, P., Jenkins, N.A., and Copeland, N.G. (2003). A highly efficient recombineering-based method for generating conditional knockout mutations. Genome Res. *13*, 476–484.

Luebben, W.R., Sharma, N., and Nyborg, J.K. (2010). Nucleosome eviction and activated transcription require p300 acetylation of histone H3 lysine 14. Proc. Natl. Acad. Sci. USA *107*, 19254–19259.

Luger, K., Rechsteiner, T.J., and Richmond, T.J. (1999). Expression and purification of recombinant histones and nucleosome reconstitution. Methods Mol. Biol. *119*, 1–16.

Miller, T.C.R., Simon, B., Rybin, V., Grötsch, H., Curtet, S., Khochbin, S., Carlomagno, T., and Müller, C.W. (2016). A bromodomain-DNA interaction facilitates acetylation-dependent bivalent nucleosome recognition by the BET protein BRDT. Nat. Commun. *7*, 13855.

Montellier, E., Boussouar, F., Rousseaux, S., Zhang, K., Buchou, T., Fenaille, F., Shiota, H., Debernardi, A., Héry, P., Curtet, S., et al. (2013). Chromatin-to-nucleoprotamine transition is controlled by the histone H2B variant TH2B. Genes Dev. *27*, 1680–1692.

Morinière, J., Rousseaux, S., Steuerwald, U., Soler-López, M., Curtet, S., Vitte, A.-L., Govin, J., Gaucher, J., Sadoul, K., Hart, D.J., et al. (2009). Cooperative binding of two acetylation marks on a histone tail by a single bromodomain. Nature *461*, 664–668.

Panne, D., McWhirter, S.M., Maniatis, T., and Harrison, S.C. (2007). Interferon regulatory factor 3 is regulated by a dual phosphorylation-dependent switch. J. Biol. Chem. *282*, 22816–22822.

Reynoird, N., Schwartz, B.E., Delvecchio, M., Sadoul, K., Meyers, D., Mukherjee, C., Caron, C., Kimura, H., Rousseaux, S., Cole, P.A., et al. (2010). Oncogenesis by sequestration of CBP/p300 in transcriptionally inactive hyperacetylated chromatin domains. EMBO J. *29*, 2943–2952.

Sasaki, K., Ito, T., Nishino, N., Khochbin, S., and Yoshida, M. (2009). Real-time imaging of histone H4 hyperacetylation in living cells. Proc. Natl. Acad. Sci. USA *106*, 16257–16262.

Schwartz, B.E., Hofer, M.D., Lemieux, M.E., Bauer, D.E., Cameron, M.J., West, N.H., Agoston, E.S., Reynoird, N., Khochbin, S., Ince, T.A., et al. (2011). Differentiation of NUT midline carcinoma by epigenomic reprogramming. Cancer Res. *71*, 2686–2696.

Shang, E., Nickerson, H.D., Wen, D., Wang, X., and Wolgemuth, D.J. (2007). The first bromodomain of Brdt, a testis-specific member of the BET sub-family of double-bromodomain-containing proteins, is essential for male germ cell differentiation. Development *134*, 3507–3515.

Sharma, N., and Nyborg, J.K. (2008). The coactivators CBP/p300 and the histone chaperone NAP1 promote transcription-independent nucleosome eviction at the HTLV-1 promoter. Proc. Natl. Acad. Sci. USA *105*, 7959–7963.

Vizcaíno, J.A., Csordas, A., del-Toro, N., Dianes, J.A., Griss, J., Lavidas, I., Mayer, G., Perez-Riverol, Y., Reisinger, F., Ternent, T., et al. (2016). 2016 update of the PRIDE database and its related tools. Nucleic Acids Res. *44* (*D1*), D447–D456.

STAR★METHODS

KEY RESOURCES TABLE

REAGENT or RESOURCE	SOURCE	IDENTIFIER
Antibodies		
Rabbit polyclonal anti-Nut	This paper	N/A
Mouse monoclonal anti-Actin	Sigma	Cat#A5441; RRID: AB_476744
Rabbit polyclonal anti-Brdt	Shang et al., 2007	N/A
Mouse monoclonal anti-H3K9ac	Active Motif	Cat#61251
Mouse monoclonal anti-H4K5ac	Active Motif	Cat#61523
Rabbit polyclonal anti-H4K5ac	Abcam	Cat#ab51977
Rabbit polyclonal anti-H4K8ac	PTM Biolabs	Cat#120
Rabbit polyclonal anti-H4K12ac	Active Motif	Cat#39165; RRID: AB_2615076
Rabbit polyclonal anti-H3	Abcam	Cat#ab1791; RRID: AB_302613
Rabbit polyclonal anti-TH2B	Abcam	Cat#ab61245
Goat polyclonal anti-TP2 (K18)	Santa Cruz	Cat#SC-21106; RRID: AB_2206859
Mouse monoclonal anti-Prm2	Briar Patch Biosciences	Cat#HUP2B; RRID: AB_2687949
Rabbit polyclonal anti-TP1	Gift by S. Kistler	N/A
Rabbit polyclonal anti-H4	Abcam	Cat#ab10158; RRID: AB_296888
Mouse monoclonal anti-Protamine P1	Briar Patch Biosciences	Cat#HUP1N; RRID: AB_2651186
Lectin PNA Alexa Fluor 647 conjugate	Life Technologies	Cat#L32460
Bacterial and Virus Strains		
EMBAC-Y baculovirus	This paper	https://geneva-biotech.com/product_category/insect-cell-expression/multibac/
Chemicals, Peptides, and Recombinant Proteins		
Complete Protease Inhibitor EDTA-free	Sigma-Aldrich	Cat#4693159001
n-Butyric Acid	Sigma-Aldrich	Cat#B-2503
Nicotinamide	Sigma-Aldrich	Cat#N-3376
nProtein A Sepharose 4 Fast Flow	GE Healthcare	Cat#17-5280-01
Trichloroacetic Acid Solution	Sigma-Aldrich	Cat#T-0699
Deposited Data		
MNase-Seq: Gene Expression Omnibus accession number: GSE111931	This paper	https://www.ncbi.nlm.nih.gov/geo/query/acc.cgi?acc=GSE111931
Raw mass spectrometry proteomics: ProteomeXchange consortium via the PRIDE partner repository; accession number: PXD008727	This paper	http://proteomecentral.proteomexchange.org/cgi/GetDataset?ID=PXD008727
Mendeley Data	This paper	https://data.mendeley.com/datasets/9xt8rgn265/draft?a=1653d1d4-ee86-4c50-b465-8ee1a0fc283a
Illumina expression raw and normalized data: Gene Expression Omnibus accession number: GSE118969	This paper	https://www.ncbi.nlm.nih.gov/geo/query/acc.cgi?acc=GSE118969
Experimental Models: Organisms/Strains		
Mouse: B6.129/SvPas-*nutm1 KO/KO*	This paper	N/A
Oligonucleotides		
RT-qPCR *Nut* forward primer: ACCTCGGATTATGGCATCAG	This paper	N/A
RT-qPCR *Nut* reverse primer: GCCAGTGCCAGGTTTCAT	This paper	N/A
Genotyping *Nut* wild-type forward primer: ACACAAGCAACAACCATGGA	This paper	N/A

(*Continued on next page*)

Continued

REAGENT or RESOURCE	SOURCE	IDENTIFIER
Genotyping *Nut KO* forward primer: AGAGGAAGTCTCCCAGCCTT	This paper	N/A
Genotyping *Nut* wild-type *and KO* reverse primer: TCTGGATTCATCGACTGTGG	This paper	N/A
Southern blot *Nut* probe forward: AAATACATGGTGGGCAGGAA	This paper	N/A
Southern blot *Nut* probe reverse: ACAGTCCTGGGCTGAGAGAA	This paper	N/A
Recombinant DNA		
cDNA sequence encoding residues 347-588 (NUT-F1C fragment) cloned in pETM30 vector with a TEV cleavable N-terminal glutathione S-transferase (GST) tag	This paper	EMBL
Software and Algorithms		
Bowtie2 v2.2.9	NA	http://bowtie-bio.sourceforge.net/bowtie2/index.shtml
Samtools v1.3.1	NA	http://samtools.sourceforge.net/
DeepTools v2.2.4	NA	https://github.com/fidelram/deepTools
GSEA	Broad Institute	http://software.broadinstitute.org/gsea/index.jsp
DANPOS v2.2.2	NA	https://sites.google.com/site/danposdoc/
R v3.3.1	R Development Core Team	https://cran.r-project.org/
Snakemake v3.9.0	NA	https://snakemake.readthedocs.io/en/latest/
Fastx-toolkit v0.0.13	NA	http://hannonlab.cshl.edu/fastx_toolkit/index.html
Xcalibur 2.1	Thermo Scientific	OPTON-20487
Mascot Distiller	Matrix Science	Version 2.6.0
Mascot Server	Matrix Science	Version 2.6.0
Proline	Open source	http://www.profiproteomics.fr/proline

CONTACT FOR REAGENT AND RESOURCE SHARING

Further information and requests for resources and reagents should be directed to and will be fulfilled by the Lead Contact, Saadi Khochbin (saadi.khochbin@univ-grenoble-alpes.fr).

EXPERIMENTAL MODEL AND SUBJECT DETAILS

Animal care and breading

Mice were housed in the Grenoble High Technology Animal Facility (PHTA, University Grenoble Alpes). For this study no experimentation was required on live animals. Mice were euthanized following a procedure approved by the official ethic committee of the University Grenoble Alpes (COMETH, C2EA-12) and all of the investigators directly involved in care and breading have an official animal-handling authorization obtained after 2 weeks of intensive training and a final formal evaluation.

Generation of Mouse: B6.129/SvPas-*nutm1*$^{KO/KO}$ (*Nut KO*)

The *nutm1*^{KO} (*Nut*^{KO}) allele was constructed as follows using the gap-repair recombineering technique adapted from (Liu et al., 2003). An 11.3-kb DNA fragment encompassing exons 1, 2, and 3 (4.7-kb upstream and 6.6-kb downstream of the start codon) of the *Nut* gene was retrieved from a BAC (bMQ 235I10, CHORI) into the SpeI-linearized PL253 retrieval plasmid after induction of recombination in SW102 electro-competent cells. Two ~0.3-kb fragments surrounding the exon 2 of the *Nut* gene (0.9-kb and 3.7-kb downstream of the start codon) were cloned into a PL452 plasmid upstream and downstream of a neomycin cassette, respectively. An *EcoR*I restriction site was inserted at the 3′end of the first fragment to facilitate the identification of the mutant allele. In order to generate the *Nut* KO targeting vector, a SalI/*Not*I fragment encompassing the neomycin cassette was purified from the *Nut* PL452-derived plasmid and cloned into the PL253 retrieval plasmid, containing the 11.3-kb DNA fragment of the *Nut* gene, after induction of recombination in SW102 cells and kanamycin selection. This strategy replaces the exon 2 of the *Nut* gene by a neomycin cassette. For gene targeting, 50 μg of *Not*I-linearized *Nut* KO targeting vector DNA (PL253) was electroporated (250V, 500 mF) into 10^7 AT1 embryonic stem cells (ESC) grown on mitomycin C-inactivated mouse embryo fibroblasts. Colonies were positively

and negatively selected in ESC medium with neomycin and ganciclovir, respectively. One hundred neomycin-resistant clones were picked and analyzed by Southern blotting using *EcoR*I digests with a 3′ external probe to check for homologous targeting (see Figure S2). Three selected ES clones were then used to generate the corresponding mouse model (Mouse B6.129/SvPas-*nutm1 KO/KO)*.

Studies were carried out on male adult mice (3 to 10 months old), except for Figures 1A and 1B, where prepubertal male mice were used from day post-partum 6 to day post-partum 50.

METHOD DETAILS

Epididymis and testis histology

Six micrometre paraffin-embedded formalin-fixed cauda epididymis sections were stained with hematoxylin. Testis sections were either processed for DAPI staining or Protamine 1 immunostaining. For details see (Gaucher et al., 2012) and (Barral et al., 2017).

Round and early elongating spermatids enrichment

Fractions enriched in spermatogenic cells at different stages of maturation, including post meiotic round and early elongating spermatids were obtained by sedimentation on a BSA gradient as detailed in a recent dedicated method publication (Buchou et al., 2017).

Histone preparation

Histone extraction was performed on germ cell nuclei of enriched round and early elongating spermatids, using 0.2 M H_2SO_4 at 4°C for 16 h followed by centrifugation at 16,000 x *g* for 10 min at 4°C to isolate solubilized histones. For germ cell preparation, see (Buchou et al., 2017). Histone precipitation was performed with TCA, 20% final concentration, added drop by drop for 30 min at 4°C and centrifuged at 16,000 x *g* for 10 min to obtain histone pellets. The pellets were washed once with cold acetone with 0.1% HCl, and twice with cold acetone. Precipitates were dried completely at room temperature.

RNA preparation and transcriptomics

RNA from testes harvested at various times after birth or from enriched round and early elongating spermatids was extracted in Trizol reagent followed by purification using the RNeasy Mini Kit (QIAGEN; for details, see (Buchou et al., 2017)). RNA was used on Illumina mouse whole-genome chip as performed in (Gaucher et al., 2012).

Protein sample preparation, western blotting

For total protein extracts, whole testes were homogenized in 8 M urea and sonicated at 250 J. Dried extracted histones were disolved in 8 M urea. Protein dosage was assessed by Bradford assay. Western blots with SDS-PAGE were carried out using the antibodies listed in Key Resource Table.

Immunofluorescence Analysis

Testes were frozen in liquid nitrogen and cut, and then gently pressed onto glass slides and air-dried. Slides were incubated in 90% ethanol during 15 min, and air-dryed again. Slides were permeabilized in 0.5% saponine, 0.2% Triton X-100, and 1x PBS at room temperature during 15 min. Saturation was performed by incubating slides in 5% dry milk, 0.2% Tween 20, and 1x PBS at room temperature for 30 min. Primary antibodies, diluted in 1% dry milk, 0.2% Tween 20, and 1x PBS, were applied onto the slides, followed by overnight incubation in a humidified chamber at 4°C, and washed 3 × 5 min in the dilution buffer. The secondary antibodies, diluted at 1:500 in the same buffer, was then applied and the slides incubated in a humidified chamber for 30 min at 37°C, and then washed as previously. After counterstaining by DAPI, the slides were mounted in Dako fluorescent mounting medium.

Antibodies' Dilutions

Rabbit polyclonal anti-Nut: 1/500 (immunoblotting), 1/25 (immunofluorescence); Mouse monoclonal anti-Actin: 1/5000 (immunoblotting); Rabbit polyclonal anti-Brdt: 1/500 (immunoblotting); Mouse monoclonal anti-H3K9ac: 1/2000 (immunoblotting); Mouse monoclonal anti-H4K5ac: 1/500 (immunofluorescence); Rabbit polyclonal anti-H4K5ac: 1/2000 (immunoblotting); Rabbit polyclonal anti-H4K8ac: 1/2000 (immunoblotting); Rabbit polyclonal anti-H4K12ac: 1/1000 (immunoblotting); Rabbit polyclonal anti-H3: 1/5000 (immunoblotting); Rabbit polyclonal anti-TH2B: 1/1000 (immunofluorescence); Goat polyclonal anti-TP2 (K18): 1/250 (immunofluorescence); Mouse monoclonal anti-Protamine P1: 1/100 (immunohistochemistry and immunofluorescence); Rabbit polyclonal anti-H4: 1/1000 (immunoblotting); Rabbit polyclonal anti-TP1, 1/500 (immunofluorescence); Mouse monoclonal anti-Prm2: 1/100 (immunofluorescence).

For precise reference regarding antibodies, please see Key Resource Table.

Recombinant protein expression

Expression and purification of Flag-tagged p300 protein (NCBI reference sequence: NM_001429.3) encoding residues 340-2094 was done as previously described (Panne et al., 2007). The procedure of p300 and NUT-p300 interacting fragment is as follows.

We used EMBAC-Y baculovirus for p300 expression. The recombinant baculoviruses were propagated in Sf21 insect cells with Sf-900 III SFM medium (Invitrogen). Hi5 insect cells (Invitrogen) in Express Five SFM medium were infected with recombinant baculovirus at a multiplicity of infection of 2, maintained in shake flasks at 27°C and harvested by centrifugation 68-72 h post infection. Cells were resuspended in lysis buffer (20 mM Tris pH 7.5, 500 mM NaCl, 5 microM $ZnCl_2$, 10 μl benzonase (SIGMA), Complete Protease Inhibitors EDTA-Free (Roche), 5% glycerol, 0.1% Tween) and sonicated. The lysate was clarified by centrifugation and applied to anti-Flag M2 affinity resin according to instructions by the manufacturer (Sigma). The resin was washed with the same buffer and the protein was eluted with buffer containing 0.2 mg/ml flag peptide and further purified by gel filtration on a Superdex 200 10/300 column (GE Healthcare) equilibrated in 20 mM HEPES buffer pH 7.5, 500 mM NaCl, 0.5 mM TCEP and 5 microM $ZnCl_2$.

For NUT expression, cDNA sequence encoding residues 347-588 (NUT-F1C fragment) was cloned into the pETM30 vector (EMBL) with a TEV cleavable N-terminal glutathione S-transferase (GST) tag. The recombinant GST-NUT fusion protein was expressed in *E. coli* BL21 (DE3) in LB medium. Cell pellets were resuspended in buffer 1 containing 20 mM Tris pH 7, 300 mM NaCl, 0.5 mM TCEP, Complete Protease Inhibitor EDTA-free (Roche) and sonicated. The lysate was clarified by centrifugation and applied to a Glutathione Sepharose 4 Fast Flow resin (GE Healthcare). The resin was washed with buffer 1 and the protein was eluted with buffer containing 20 mM Glutathione. The protein was further purified by gel filtration in buffer 1 on a Superdex 75 10/300 GL column (GE Healthcare).

Recombinant *Xenopus laevis* histones H2A, H2B, H3 and H4 were expressed, purified and refolded according to standard procedures (Luger et al., 1999). Histone octamers were assembled by mixing equimolar amounts of each histone subunit. After mixing H2A, H2B, H3 and H4, the sample was incubated for one hour on ice then run on Superdex 75 10/300 GL size exclusion column in refolding buffer (10 mM Tris pH 7.5, 2M NaCl, 1 mM EDTA, 5 mM β-mercaptoethanol). All preparations were confirmed by SDS-PAGE and mass spectrometry.

In vitro Histone acetyltransferase assays

Histone octamer acetylation reactions were performed in acetylation buffer (20 mM Tris pH 7.5, 100 mM NaCl, 1 mM DTT, 10% glycerol and Complete Protease Inhibitor EDTA-free (Roche)) with 100 microM Acetyl-CoA, 2 μg of p300, 4 μg of purified histone octamers in the presence or absence of 4 μg of GST-NUT-F1C (p300:NUT, 1:10 molar stoichiometry). Control experiments were performed with NUT-F1C and histone octamers. The reactions were incubated for one hour at 30°C and stopped by addition of 1X SDS Laemmli buffer. The samples were then analyzed by SDS-PAGE and mass spectrometry.

Proteomics of histone modifications

Digestion and chemical derivatization

For histone peptides with no chemical derivatization, the sample was digested with trypsin at 37°C overnight. For stable chemical isotope labeling samples, chemical derivatization was carried out as described previously (Garcia et al., 2007). Twenty micrograms of each histone sample were propionylated with C_{12} or C_{13} propionic anhydride in buffer (100 mM NH_4HCO_3, 100 mM $NaHCO_3$, pH 8.0) at 37°C for one hour, and the propionylation reaction was then repeated. The sample was then digested with trypsin at 37°C overnight. After digestion, N-terminal of tryptic peptides were further propionylated with C_{12} or C_{13} propionic anhydride, respectively. The light and heavy labeling peptides were then mixed, and subjected to MS analysis.

Nano-HPLC-MS/MS analysis

Peptides were injected onto a manually packed reversed phase C18 column (170 mm × 79 microm, 3-microm particle size, Dikma, China) connected to an Easy-nLC 1000 chromatography system (Thermo Fisher Scientific, Waltham, MA). Peptides were dissolved in solvent A (0.1% formic acid in 2% acetonitrile and 98% H_2O) and eluted using a 2-h gradient of 8% to 80% solvent B (0.1% formic acid in 90% acetonitrile and 10% H_2O) at a flow rate of 300 nl/min, and analyzed by an Orbitrap Fusion mass spectrometer (Thermo Fisher Scientific, San Jose, CA). The full MS range was set from *m/z* 350 to 1800 with a resolution of 240,000 at *m/z* 400. For MS/MS scans, the twenty most intense ions with intensity greater than 5,000 and charge states of +1, +2, or +3 in each full MS spectrum were sequentially fragmented in a linear ion trap by collision-induced dissociation, using a normalized collision energy of 35%. The dynamic exclusion duration was set to 15 s, and the isolation window was 1.5 m/z. All histone samples were analyzed twice.

Mass spectrometric data analysis

All acquired MS raw files were transformed into MGF format by Proteome Discoverer software (version 1.4, Thermo Fisher Scientific, Waltham, MA), then all MGF files were analyzed by Mascot software (version 2.3.01, Matrix Science Ltd., London, UK) against a mouse histone sequence database (94 sequences, 14,024 residues, updated on 05/07/2014) generated in-house from the UniProt database. For stable isotope labeling, propionyl (N-terminal of peptide), propionyl_C13 (N-terminal of peptide), propionyl (K), propionyl_C13 (K), propionylation-methylation (K), propionylation_C13-methylation (K), dimethyl (K), trimethyl (K), and acetyl (K) were specified as variable modifications. For histone peptides with no chemical derivatization, acetyl (K), methyl (KR), dimethyl (KR) and trimethyl (K) were specified as variable modifications. Other parameters for all analyses were specified as follows: mass error was ± 10 ppm for parent ions and ± 0.5 Da for fragment ions. The enzyme was specified as trypsin with a maximum of 5 missing cleavages. Peptide ion score cut-off was 20, and the spectra of all identified peptides were checked manually according to criteria reported previously to ensure the accuracy of peptide identification (Chen et al., 2005).

Quantification of histone PTMs

Identified peptides bearing modifications were manually quantified using the QualBrowser version 3.0.63 (Thermo Fisher Scientific). Extracted ion chromatograms were constructed for each precursor m/z value with a mass tolerance of 10 ppm and mass precision up

to four decimal places. For stable isotope labeling, peak areas for a pair of heavy and light peptides with the same retention time interval were calculated. Precursor ion AUC of prDNIQGITKprPAIR for H4, prEIAQDFKprTDLR for H3, prIASEASR for H2B and prAGLQFPVGR for H2A were used to normalize the amount of each histone in stable isotope labeling quantification. For histone peptides with no chemical derivatization, precursor ion AUC of YRPGTVALR, STELLIR, EIAQDFK, DNIQGITKPAIR, ISGLIYEETR were used to normalize the amount of each histone. Two technical replicates were used to quantify histone marks.

For the identification and quantification of histone acetylation following *in vitro* HAT with p300, we followed the previously published procedure (Goudarzi et al., 2016). See also the legend of Figure 6D.

Proteomics of Nut interactome

Immunoprecipitation of Nut

Soluble extracts of enriched round and early elongating spermatids from wild-type and *Nut KO* mice (5.10^6 cells) were obtained in $LSBD^{500}$ (50 mM HEPES pH 7, 3 mM $MgCl_2$, 500 mM KCl, 20% Glycerol, 1mM DTT, 100 ng/ml TSA, Protease Cocktail Inhibitor). Extracts were immediately diluted with an equal volume of $LSBD^0$ (no KCl) buffer and incubated with 2.5 μg of purified anti-Nut antibody for 16h at 4°C followed by incubation with protein A Sepharose beads for 6h at 4°C under rotation. After two washing steps in $LSBD^{250}$ (250 mM KCl) buffer and two with PBS, 1 mM DTT, 100 ng/ml TSA, Protease Cocktail Inhibitor, proteins were eluted by boiling in Laemmli buffer. After separation in SDS-PAGE and staining in Coomassie blue, each sample was cut in 6 pieces for MS-based analyses.

Mass spectrometric data analysis

Proteins were in-gel digested using modified trypsin (Promega, sequencing grade) as previously described (Casabona et al., 2013). Resulting peptides were analyzed by online nanoLC-MS/MS (UltiMate 3000 and LTQ-Orbitrap Velos Pro, Thermo Scientific). For this, peptides were sampled on a 300 μm x 5 mm PepMap C18 pre-column and separated on a 75 μm x 250 mm C18 column (PepMap, Thermo Scientific). MS and MS/MS data were acquired using Xcalibur (Thermo Scientific). Peptides and proteins were identified using Mascot (version 2.6.0) through concomitant searches against Uniprot (*Mus musculus* taxonomy, August 2017 version), classical contaminants database (homemade) and the corresponding reversed databases. The Proline software (http://www.profiproteomics.fr/proline) was used to filter the results (conservation of rank 1 peptides, peptide identification FDR < 1% as calculated on peptide scores by employing the reverse database strategy, minimum peptide score of 25, and minimum of 1 specific peptide per identified protein group) before performing a compilation, grouping and comparison of the protein groups from the different samples. Proteins were considered as potential partners of the bait if they were identified only in the positive co-IPs with a minimum of 3 specific spectral counts or enriched at least 5 times in positive co-IPs compared to control ones on the basis of weighted spectral counts.

The mass spectrometry proteomics data have been deposited to the ProteomeXchange Consortium via the PRIDE (Vizcaíno et al., 2016) partner repository with the dataset identifier PXD008727.

QUANTIFICATION AND STATISTICAL ANALYSIS

Statistics and quantifications

Figure 1A, the histograms show the average values of 4 experiments ± standard deviations.

Figure 2A, right panels, the histograms show the average values ± standard deviations of litter sizes and testis weights. The average litter sizes were obtained after crossing wild-type female mice with wild-type (n = 12) or *Nut KO* (n = 5) male mice. The average weights of testes of wild-type (n = 16) and *Nut KO* (n = 19) mice were determined.

Figure 4 shows the results of two independent experiments. For each experiment round spermatid fractions were prepared from 3 (wild-type) or 5 (*KO*) mice (6 to 10 testes).

Figures 5 and 6C each shows the results of two independent experiments. For each experiment round spermatid fractions were prepared from 5 (wild-type) or 7 (*KO*) mice (10 to 14 testes).

RNAs for transcriptomic analyses (Figure 6A) were prepared from three independent experiments corresponding to three independent cell fractionations for each genotype. For each fractionation, cell suspensions from testes from two wild-type mice or three *Nut KO* mice were used. For each genotype (wild-type and *Nut KO*), 6 samples were prepared as follows. Samples 1, 2 and 3 were directly prepared from the three above-mentioned fractionations and three additional samples were obtained by respectively mixing samples 1 with 2, 2 with 3, and 1 with 3 (from left to right).

The Nut regulated genes (genes downregulated and upregulated in *Nut KO* cells compared to wild-type cells) correspond to genes showing an absolute value of fold change above 1.5 between *Nut KO* versus wild-type cells, with an adjusted Student test p value less than 5%. The Student test p values for fold changes were adjusted for multiples tests according to the method published by Benjamini & Hochberg.

Nucleosomal DNA length determination

Nuclei from fractionated round-elongating spermatids (equivalent of 100 μg of chromatin) were extensively digested with MNase. Digestion conditions were setup to completely digest chromatin to monomers. DNA was then prepared by the digestion of proteins by proteinase K in a SDS buffer and Phenol/Chloroform extraction.

Paired-end sequencing 2*75bp was performed using Illumina NextSeq 500. Base calling was performed using RTA version 2. MNase-Seq fragments were aligned to the mm10 genome assembly using Bowtie version 2.2.9 with default arguments.

Fragment sizes were taken from the 9th column of SAM files (TLEN) using Samtools version 1.3.1 and plotted as distributions using R version 3.3.1.

DATA AND SOFTWARE AVAILABILITY

Data Resources

The accession number for the raw and processed MNase sequencing data reported in this paper is GEO: GSE111931.

The accession number for the raw and processed transcriptomic Illumina data reported in this paper is GEO: GSE118969.

Proteomic data: the list of all identified proteins immunoprecipitated by the anti-Nut antibody has been deposited with ProteomeXchange consortium via the PRIDE database with the accession number: PXD008727.

ADDITIONAL RESOURCES

Anti Nut-purified antibody

5 cDNA "fragments" covering the entire mouse *Nut* sequence (Reynoird et al., 2010), were used to produce the corresponding biotinylated peptides, which were injected to rabbits. Sera from final bleedings were differently screened for a ~150kDa signal by western blotting using total germ cell lysed in 15mM Tris HCl pH 7.4, 60mM KCl, 15mM NaCl, 0.34M Sucrose, 2mM EDTA, 0.5mM EGTA, 0.65mM Spermidine, 1mM Dithiothreitol, 0.03% Triton X-100, 1% Glycerol, Protease Cocktail Inhibitor 10mM Na Butyrate, followed by centrifugation for 15 min at 200 x g at 4°C in order to obtain nuclear extracts from testis of wild-type versus *Nut KO* male mice.

Positive samples were immunopurified against the Nut f1c fragment (Reynoird et al., 2010), bound to CNBr-activated Sepharose 4B beads, after elution with 0.1M Glycine pH2.5. Purified antibodies were dialysed and concentrated in a PBS, 350mM NaCl, 10% glycerol buffer at 0.5 μg/microliter and kept at −20°C until use.

Cell Reports, Volume *24*

Supplemental Information

Nut Directs p300-Dependent, Genome-Wide H4 Hyperacetylation in Male Germ Cells

Hitoshi Shiota, Sophie Barral, Thierry Buchou, Minjia Tan, Yohann Couté, Guillaume Charbonnier, Nicolas Reynoird, Fayçal Boussouar, Matthieu Gérard, Mingrui Zhu, Lisa Bargier, Denis Puthier, Florent Chuffart, Ekaterina Bourova-Flin, Sarah Picaud, Panagis Filippakopoulos, Afsaneh Goudarzi, Ziad Ibrahim, Daniel Panne, Sophie Rousseaux, Yingming Zhao, and Saadi Khochbin

Supplemental Figures and Tables

Supplemental information includes 5 Figures and 5 Tables.

Shiota_Figure S1 (related to Figure 1)

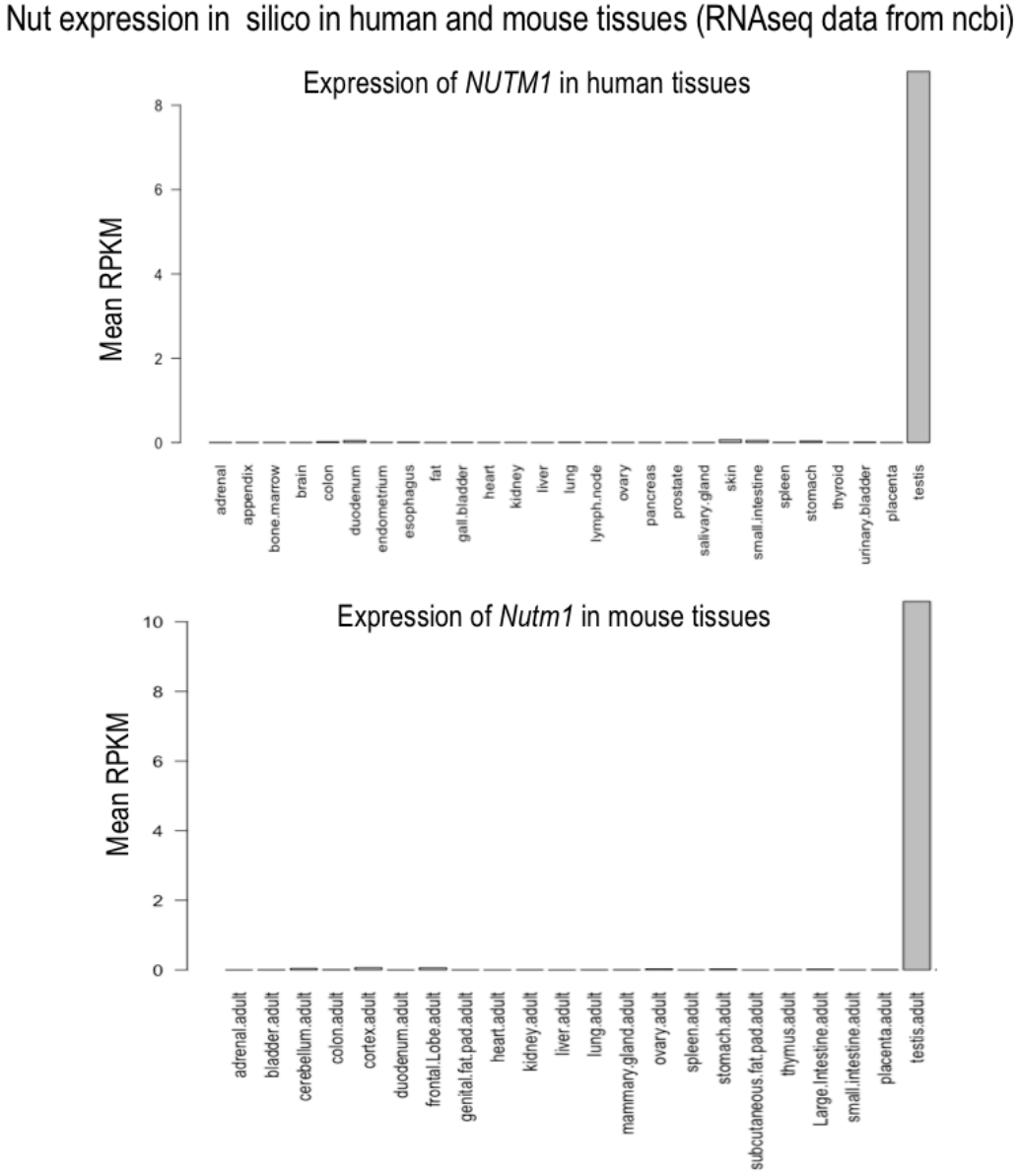

Figure S1 (related to Figure 1)

NUT/*Nut* is a testis-specific gene

Using publicly available normalized RNAseq data from 22 mouse (https://www.ncbi.nlm.nih.gov/bioproject/PRJNA66167/) and 27 human (https://www.ncbi.nlm.nih.gov/bioproject/PRJEB4337/) adult normal tissues, the tissue-specific expression of *Nut*/*NUT* is visualized. Related to Figure 1A.

Shiota_Figure S2 (related to Figure 2)

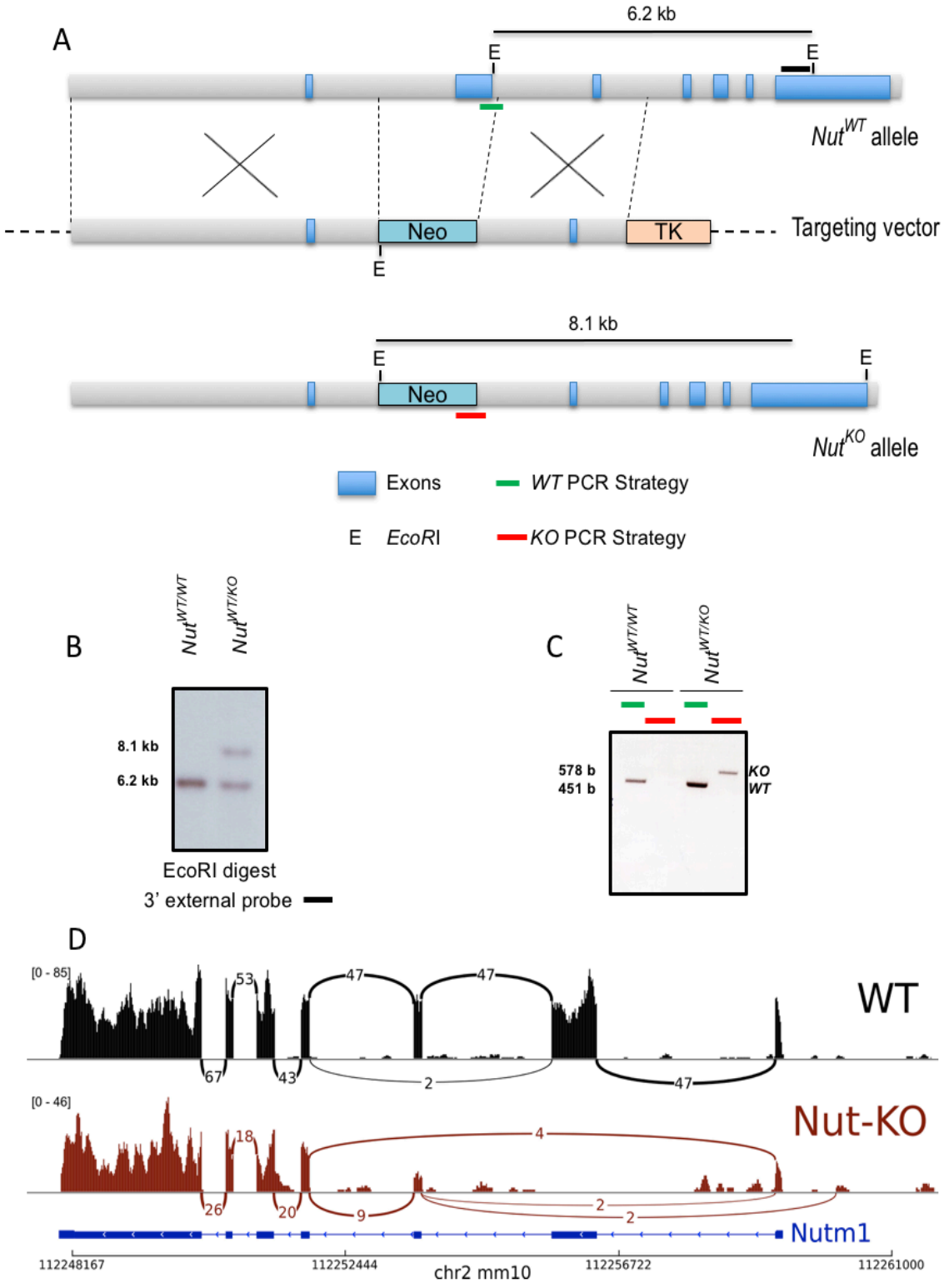

Figure S2 (related to Figure 2)

Generation of *Nut KO* mice

(A) Strategy to inactivate *nutm1* (*Nut*) by inserting a *Neo* cassette instead of the second exon and validation of the insertion event by Southern blotting (B) and PCR (C). The positions of the probe used in the Southern blot analysis and the regions amplified by PCR are indicated. (D) To control the result of our genetic manipulations, we also sequenced RNAs from *WT* and *Nut KO* round/elongating spermatids from one of the cell fractionations described in the legend of Figure 6A. The alignment of RNA-seq reads from *WT* and *Nut KO* round/elongating spermatids shows the disruption of *Nut* transcription in *Nut KO* cells. Sashimi plots represent the raw RNAseq coverage around *Nut* genomic coordinates. Arcs show junction events in reads. Values are the number of junction reads for their relative arc. Junction events occurring only once are not displayed.

Shiota_Figure S3 (related to Figure 3)

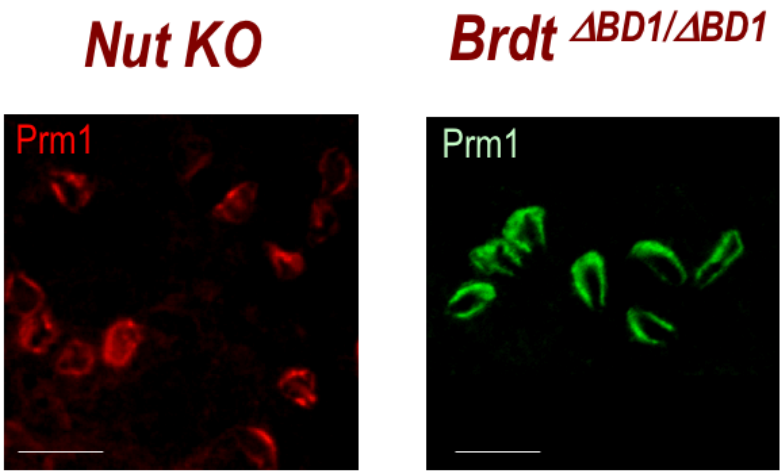

Figure S3 (related to Figure 3)

Similar impairment of protamine assembly is observed in *Nut KO* as in *Brdt*$^{deltaBD1/deltaBD1}$ condensing spermatids. The left and right panels show condensing spermatids in testes from *Nut KO* and *Brdt*$^{deltaBD1/deltaBD1}$ respectively (Gaucher et al., 2012) after immunodetection of protamine 1 (Prm1) as indicated. Note that different colours are used to detect Prm1 in the two preparations. Scale bar: 10 micrometres.

Shiota_Figure S4 (related to Figure 6)

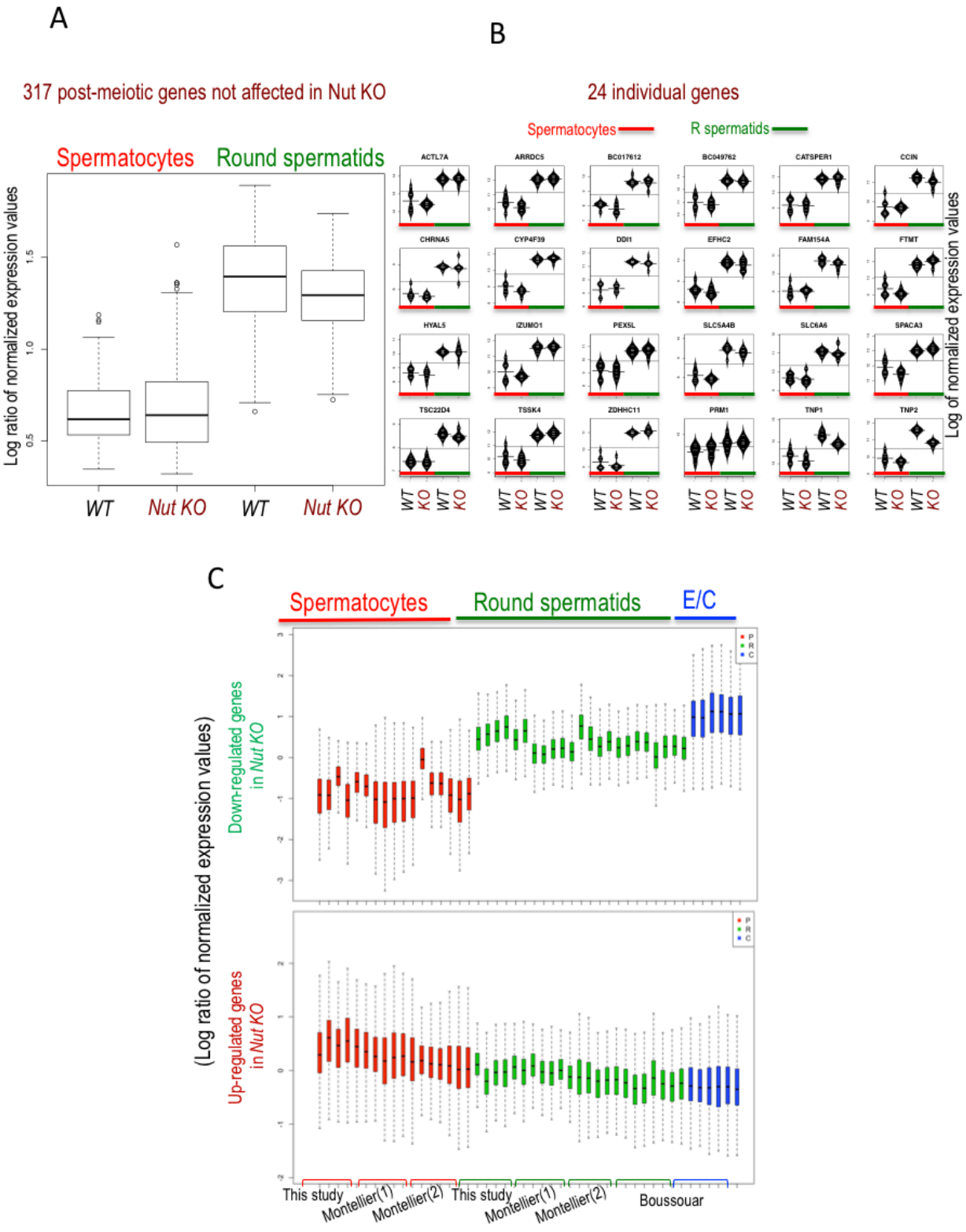

Figure S4 (related to Figure 6A)

Nut activates the expression of post-meiotic genes.

(A) and (B) show the expression of genes not affected by Nut, that are up-regulated in post-meiotic cells in *WT* cells and their expression in *Nut KO* cells.

(A) Quality control of *WT* and *Nut KO* spermatocytes and round/early elongating spermatid fractions. In order to confirm that post-meiotic *WT* and *Nut KO* populations are comparable, the global expression of 317 genes that are activated in post-meiotic cells compared to spermatocytes, was monitored. Nut regulated genes (shown in C) were excluded from this list of genes.

(B) Expression of 24 individual genes within the genes whose expression is globally shown in (A). The expression of 21 individual post-meiotic genes in both *WT* and *Nut KO* cell populations is shown. The expression of Prm1, TP1 and TP2-encoding genes is also shown. It is of note that the Illumina microarray used does not include probes for Prm2 expression.

(C) Expression of Nut regulated genes during spermatogenesis. The expression profiles during spermatogenic cells differentiation of the genes identified here as Nut-regulated genes by the comparative analysis of transcriptomes between *WT* and *Nut KO* round/elongating spermatids (Fig. 6A), was visualized. For this purpose, we used independent stage-specific transcriptomic data previously generated from *WT* germ cells (Boussouar et al., 2014; Montellier et al., 2013) as well as in the present study as indicated. Montellier (1) and Montellier (2) correspond to the *WT* cells of two different experiments, respectively used to compare with germ cells of *TH2B KO* and *Th2Btag* mutated mice (Montellier et al. 2013). The upper panel shows the stage-specific expression of genes whose expression are down-regulated in the absence of Nut and the lower panel shows genes whose expression are upregulated in *Nut KO* cells. The stages are colour coded as indicated. E/C means elongating/condensing spermatids.

Shiota_Figure S5 (related to Figure 6)

A

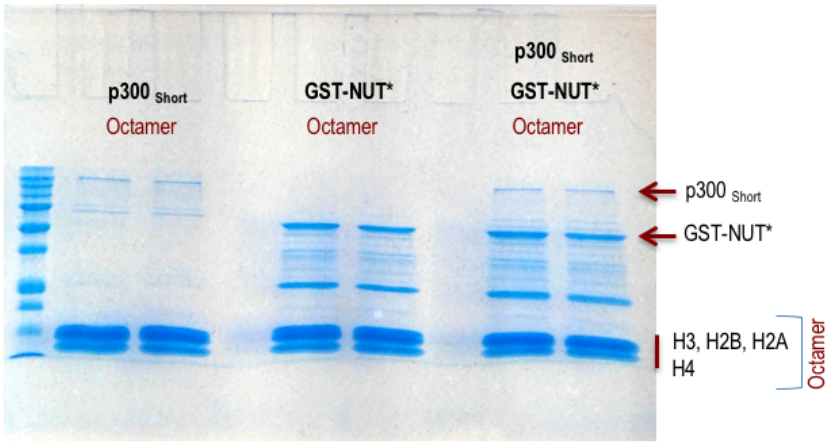

B

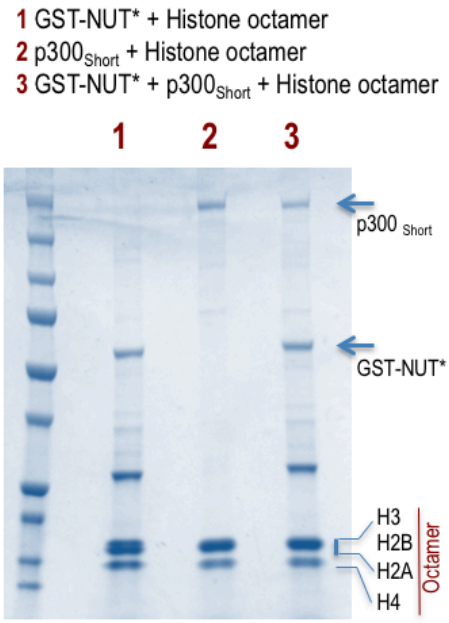

C

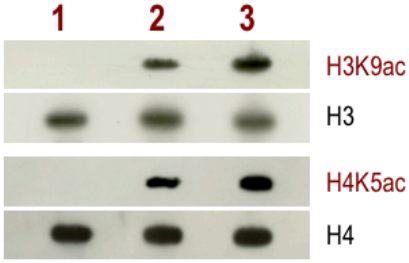

Figure S5 (related to Figure 6D)

NUT mediates the stimulation of H4 acetylation by p300.

(A) Coomassie stained gel corresponding to each reaction and the histones prior to the HPLC/MS/MS analysis. This panel shows the Coomassie gel staining of proteins used in the HAT assays presented in Figure 6D is shown. Histone-containing regions of the gel were cut and used for further analysis by mass spectrometry (Fig. 6D). $p300_{short}$ corresponds to residues 340-2094 of p300. GST-NUT* corresponds to residues 347-588 of NUT, previously shown to interact with p300 (Reynoird et al., 2010).

(B) and (C) correspond to an experiment similar to the one shown in Fig. 6D, except that the acetylation of H3K9ac and H4K5ac was monitored by specific antibodies.

(B) A fraction of the experiment described above was analysed by SDS-PAGE and stained by Coomassie.

(C) Another fraction of the experiment performed in (B) was used to detect the indicated histone acetylation. H3 and H4 were also detected with the corresponding antibodies as indicated.

Shiota_Table S1 (related to Fig. 5A)

No	Modifications	Replications	Ratio Nut-/-/WT (Normalized)	Average Ratio Nut-/-/WT (Normalized)
1	H3K14ac	1	0.81	0.79
	H3K14ac	2	0.77	
2	H3K18ac	1	0.93	0.90
	H3K18ac	2	0.87	
3	H3K23ac	1	0.97	0.93
	H3K23ac	2	0.89	
4	H4K5ac	1	0.31	0.32
	H4K5ac	2	0.33	
5	H4K8ac	1	0.45	0.44
	H4K8ac	2	0.43	
6	H4K12ac	1	1.17	1.10
	H4K12ac	2	1.04	
7	H4K16ac	1	0.66	0.64
	H4K16ac	2	0.62	
8	H2AK5ac (Isoform,Uniprot No.A0AUV1)	1	0.40	0.39
	H2AK5ac (Isoform,Uniprot No.A0AUV1)	2	0.37	
9	H2AK9ac (Isoform,Uniprot No.A0AUV1)	1	0.40	0.39
	H2AK9ac (Isoform,Uniprot No.A0AUV1)	2	0.37	
10	H2AK74ac (Isoform,Uniprot No.A0AUV1)	1	0.92	0.93
	H2AK74ac (Isoform,Uniprot No.A0AUV1)	2	0.94	

Table S1 (related to Figure 5A)

Relative quantitative analysis of site-specific histone acetylation in *WT* round/elongating spermatids compared to their *Nut KO* counterpart.

All the identified peptides with Mascot score above 20 were manually verified according to the rules described previously (Chen et al., 2005). The relative ratios of abundance of histone peptides in *WT* and *Nut KO* histone samples were calculated by the peak area of the light and heavy isotope peaks. The PTM with more than 1.5 times variations are indicated in red (see Table S2 for details).

Shiota_Table S2 (related to Fig. 5A)

No	Modifications	Replications	Sequence	Peak area		Ratio Nut^{+}/WT	Ratio Nut^{+}/WT (Normalized)	Average Ratio Nut^{+} /WT (Normalized)
				Nut	WT			
1	H3K14ac	1	pr-K(me2)STGGK(ac)APR	2.22E+07	2.97E+07			
		2		1.49E+08	2.05E+08			
		1	pr-K(pr)STGGK(ac)APR	3.69E+07	5.76E+07			
		2		7.67E+08	1.10E+09			
		1	pr-K(me3)STGGK(ac)APR	3.91E+07	5.12E+07			
		2		2.60E+08	3.43E+08			
	SUM	1		9.82E+07	1.39E+08	0.71	0.81	0.79
		2		1.18E+09	1.65E+09	0.71	0.77	
2	H3K18ac	1	pr-K(ac)QLATK(ac)AAR	4.96E+07	5.64E+07			
		2		7.67E+08	8.61E+08			
		1	ac)QLATK(pr)AAR or pr-K(pr)QLATK(ac)	3.37E+08	3.96E+08			
		2		5.01E+09	6.14E+09			
		1	pr-K(ac)QLATK(me1+pr)AAR	8.11E+08	1.01E+09			
		2		1.52E+10	1.88E+10			
	SUM	1		1.20E+09	1.46E+09	0.82	0.93	0.90
		2		2.10E+10	2.58E+10	0.81	0.87	
3	H3K23ac	1	pr-K(ac)QLATK(ac)AAR	4.96E+07	5.64E+07			
		2		7.67E+08	8.61E+08			
		1	ac)QLATK(pr)AAR or pr-K(pr)QLATK(ac)	3.37E+08	3.96E+08			
		2		5.01E+09	6.14E+09			
	SUM	1		3.86E+08	4.52E+08	0.85	0.97	0.93
		2		5.78E+09	7.00E+09	0.82	0.89	
4	H4K5ac	1	pr-GK(ac)GGK(pr)GLGK(pr)GGAK(pr)R	NA	6.36E+07			
		2		NA	4.59E+08			
		1	pr-GK(ac)GGK(ac)GLGK(pr)GGAK(ac)R	1.84E+07	4.69E+07			
		2		1.65E+08	3.78E+08			
		1	pr-GK(ac)GGK(pr)GLGK(ac)GGAK(ac)R	3.67E+07	9.39E+07			
		2		3.30E+08	7.56E+08			
		1	pr-GK(ac)GGK(ac)GLGK(ac)GGAK(ac)R	1.01E+06	4.35E+06			
		2		5.38E+07	2.04E+08			
	SUM	1		5.61E+07	2.09E+08	0.27	0.31	0.32
		2		5.48E+08	1.80E+09	0.30	0.33	
5	H4K8ac	1	pr-GK(pr)GGK(ac)GLGK(pr)GGAK(pr)R	NA	3.81E+08			
		2		NA	2.76E+09			
		1	pr-GK(pr)GGK(ac)GLGK(ac)GGAK(pr)R	1.78E+08	6.36E+07			
		2		1.28E+09	4.59E+08			
		1	pr-GK(ac)GGK(ac)GLGK(pr)GGAK(ac)R	1.84E+07	4.69E+07			
		2		1.65E+08	3.78E+08			
		1	pr-GK(pr)GGK(ac)GLGK(ac)GGAK(ac)R	1.84E+07	4.69E+07			
		2		1.65E+08	3.78E+08			
		1	pr-GK(ac)GGK(ac)GLGK(ac)GGAK(ac)R	1.01E+06	4.35E+06			
		2		5.38E+07	2.04E+08			
	SUM	1		2.16E+08	5.43E+08	0.40	0.45	0.44
		2		1.66E+09	4.18E+09	0.40	0.43	
6	H4K12ac	1	pr-GK(pr)GGK(pr)GLGK(ac)GGAK(pr)R	6.12E+08	6.62E+08			
		2		5.94E+09	6.66E+09			
		1	pr-GK(pr)GGK(pr)GLGK(ac)GGAK(ac)R	1.78E+08	6.36E+07			
		2		1.28E+09	4.59E+08			
		1	pr-GK(pr)GGK(ac)GLGK(ac)GGAK(pr)R	1.78E+08	6.36E+07			
		2		1.28E+09	4.59E+08			
		1	pr-GK(ac)GGK(pr)GLGK(ac)GGAK(pr)R	NA	6.36E+07			
		2		NA	4.59E+08			
		1	pr-GK(pr)GGK(ac)GLGK(ac)GGAK(ac)R	1.84E+07	4.69E+07			
		2		1.65E+08	3.78E+08			
		1	pr-GK(ac)GGK(pr)GLGK(ac)GGAK(ac)R	3.67E+07	9.39E+07			
		2		3.30E+08	7.56E+08			
		1	pr-GK(ac)GGK(ac)GLGK(ac)GGAK(ac)R	1.01E+06	4.35E+06			
		2		5.38E+07	2.04E+08			
	SUM	1		1.02E+09	9.98E+08	1.03	1.17	1.10
		2		9.04E+09	9.38E+09	0.96	1.04	
7	H4K16ac	1	pr-GK(pr)GGK(pr)GLGK(pr)GGAK(ac)R	1.02E+09	1.55E+09			
		2		9.89E+09	1.55E+10			
		1	pr-GK(pr)GGK(ac)GLGK(pr)GGAK(ac)R	NA	3.81E+08			
		2		NA	2.76E+09			
		1	pr-GK(pr)GGK(pr)GLGK(ac)GGAK(ac)R	1.78E+08	6.36E+07			
		2		1.28E+09	4.59E+08			
		1	pr-GK(ac)GGK(ac)GLGK(pr)GGAK(ac)R	1.84E+07	4.69E+07			
		2		1.65E+08	3.78E+08			
		1	pr-GK(pr)GGK(ac)GLGK(ac)GGAK(ac)R	1.84E+07	4.69E+07			
		2		1.65E+08	3.78E+08			
		1	pr-GK(ac)GGK(pr)GLGK(ac)GGAK(ac)R	3.67E+07	9.39E+07			
		2		3.30E+08	7.56E+08			
		1	pr-GK(ac)GGK(ac)GLGK(ac)GGAK(ac)R	1.01E+06	4.35E+06			
		2		5.38E+07	2.04E+08			
	SUM	1		1.27E+09	2.18E+09	0.58	0.66	0.64
		2		1.19E+10	2.05E+10	0.58	0.62	
8	H2AK5ac	1	pr-GK(ac)QGGK(pr)AR	7.96E+06	2.28E+07	0.35	0.40	0.39
		2		9.62E+07	2.77E+08	0.35	0.37	
9	H2AK9ac	1	pr-GK(pr)QGGK(ac)AR	3.98E+06	1.14E+07	0.35	0.40	0.39
		2		4.81E+07	1.38E+08	0.35	0.37	
10	H2AK74ac	1	pr-DNK(ac)K(me1+pr)TR	4.43E+07	5.48E+07	0.81	0.92	0.93
		2		8.81E+08	1.01E+09	0.87	0.94	

Normalization Nut^{+}/WT

Replications	1	2
H3 EIAQDFKTDLR	0.94727342	0.98400088
H4 DNIQGITKPAIR	0.88541447	0.875149837
H2A AGLQFPVGR	0.85164992	0.923494784
H2B IASEASR	0.83705144	0.92946393
Average	0.88034731	0.928027358

Coverage of Histone

Replications	1	2
H3	64%	67%
H4	93%	87%
H2A	52%	52%
H2B	48%	48%

Table S2 (related to Figure 5A)

Detailed quantitative analysis of site-specific histone acetylation in *WT* round/elongating spermatids compared to their *Nut KO* counterpart shown in Table S1. The small Table entitled "Normalization *Nut*$^{-/-}$/WT" shows the values of the precursor ion AUC used to normalize the amount of each histone in stable isotope labelling quantification. The lowest Table indicates the values of histone coverage for each experiment.

Shiota_Table S3 (related to Fig. 6C)

Protein set id	Gene name	title	Coverage	Mol. Weight	WT1_KO	WT2_KO	KO_Pep	KO_SC	KO_SSC	KO_WSC	WT1_Pep	WT1_SC	WT1_SSC	WT1_WSC	WT2_Pep	WT2_SC	WT2_SSC	WT2_WSC
Nutm1	NUT family member 1	Q8BHP2	21.58	120686	WT1 only	WT2 only					13	14	14	14	11	12	12	12
HATs																		
Crebbp	CREB-binding protein	P45481	5.9	265494	5.42	6.42	2	2	2	2	10	11	10	10.83	11	13	12	12.83
Ep300	Histone acetyltransferase p300	B2RWS6	1.95	263305	WT1 only	WT2 only					3	3	2	2.17	4	4	3	3.17
Histones, chromatin binding and transcription factors																		
Hist1h2ba	Histone H2B type 1-A (TH2B)	P70696	63.78	14236	8.89	11.10	1	1	0	0.87	6	8	6	7.73	7	10	7	9.66
H2afb1	Histone H2A-Bbd type 1 (H2AL2)	Q9CQ70	19.82	12842	WT1 only	WT2 only					2	2	2	2	2	2	2	2
H2afv	Histone H2A.V (H2AZ2)	Q3THW5	14.84	13508	8.09	7.06	1	1	0	0.33	2	6	1	2.67	2	5	1	2.33
H1fnt	Testis-specific H1 histone	Q8CJI4	9.55	44400	WT1 only	WT2 only					3	3	3	3	1	1	1	1
Hmgb4	High mobility group protein B4	Q6P8W9	12.15	21604	WT1 only	WT2 only					2	2	2	2	1	1	1	1
Tnp2	Nuclear transition protein 2	P11378	17.95	13130	WT1 only	WT2 only					1	1	1	1	1	1	1	1
Baz2a	Bromodomain adjacent to zinc finger domain protein 2A	Q91YE5	1.96	209618	WT1 only	WT2 only					2	2	2	2	2	2	2	2
Smarca5	SWI/SNF-related matrix-associated actin-dependent regulator of chromatin subfamily A me	Q91ZW3	9.42	121627	8.00	6.00	1	1	1	1	8	8	8	8	6	6	6	6
Cenpp	Centromere protein P	Q9CZ92	7.34	33287	WT1 only	WT2 only					2	2	2	2	2	2	2	2
Safb	Scaffold attachment factor B1	D3YXK2	7.26	105103	WT1 only	WT2 only					4	4	4	4	1	1	1	1
Sltm	SAFB-like transcription modulator	Q8CH25	4.75	116919	WT1 only	WT2 only					3	4	4	4	3	4	4	4
Gemin2	Gem-associated protein 2	Q9CQQ4	4.46	30441	WT1 only	WT2 only					1	1	1	1	1	2	2	2
Dot1l	Histone-lysine N-methyltransferase, H3 lysine-79 specific (Fragment)	F7CVL0	0.83	128714	WT1 only	WT2 only					1	1	1	1	1	1	1	1
Naa40	N-alpha-acetyltransferase 40	Q8VE10	5.06	27229	WT1 only	WT2 only					1	1	1	1	1	1	1	1
Rpap3	RNA polymerase II-associated protein 3	Q9D706	3.18	74095	WT1 only	WT2 only					1	1	1	1	1	1	1	1
Sox30	Transcription factor SOX-30	Q8CGW4	1.66	83938	WT1 only	WT2 only					1	1	1	1	1	1	1	1
Ccar1	Cell division cycle and apoptosis regulator protein 1	Q8CH18	3.32	132060	WT1 only	WT2 only					3	4	4	4	1	3	3	3
Pura	Transcriptional activator protein Pur-alpha	P42669	38.63	34883	WT1 only	WT2 only					5	6	5	5.53	6	6	4	5.06
Cdc5l	Cell division cycle 5-like protein	Q6A068	5.61	92189	WT1 only	WT2 only					2	2	2	2	3	3	3	3
Pa2g4	Proliferation-associated protein 2G4	P50580	4.31	43698	WT1 only	WT2 only					2	2	2	2	1	1	1	1
Naca	Nascent polypeptide-associated complex subunit alpha, muscle-specific form	P70670	1.33	220499	WT1 only	WT2 only					2	2	2	2	2	2	2	2
Ddx17	Probable ATP-dependent RNA helicase DDX17	Q501J6	16	72399	10.89	5.07	3	3	0	0.45	10	10	4	4.9	4	4	2	2.28
Trim27	Zinc finger protein RFP	Q62158	2.34	58512	WT1 only	WT2 only					1	1	1	1	1	1	1	1
Rbbp6	E3 ubiquitin-protein ligase RBBP6	P97868	3.13	199587	WT1 only	WT2 only					2	2	2	2	3	3	3	3
Khdrbs1	KH domain-containing, RNA-binding, signal transduction-associated protein 1	Q60749	3.16	48371	WT1 only	WT2 only					1	1	1	1	1	1	1	1
Rnf17	RING finger protein 17	Q99MV7	1.71	185599	WT1 only	WT2 only					2	2	2	2	2	2	2	2
Nuclear pore complex																		
Kpnb1	Importin subunit beta-1	P70168	5.25	97184	WT1 only	WT2 only					3	3	3	3	4	4	4	4
Kpna6	Importin subunit alpha-7	O35345	9.51	59964	WT1 only	WT2 only					3	3	3	3	1	1	1	1
Nup35	Nucleoporin NUP53	Q8R4R6	4	34785	WT1 only	WT2 only					1	1	1	1	1	1	1	1
Nup210l	Nuclear pore membrane glycoprotein 210-like	Q9D2F7	0.64	208699	WT1 only	WT2 only					1	1	1	1	1	1	1	1
Nup93	Nuclear pore complex protein Nup93	Q8BJ71	2.93	93281	WT1 only	WT2 only					1	1	1	1	2	2	2	2
Splicing																		
Srpk1	SRSF protein kinase 1	O70551	9.57	73088	WT1 only	WT2 only					3	5	5	5	4	4	4	4
Srpk2	SRSF protein kinase 2	O54781	1.76	76756	WT1 only	WT2 only					1	2	2	2	1	1	1	1
Cpsf1	Cleavage and polyadenylation specificity factor subunit 1	Q9EPU4	3.19	160818	WT1 only	WT2 only					5	5	5	5	1	1	1	1
Sf3b4	Splicing factor 3B subunit 4	Q8QZY9	8.96	44355	WT1 only	WT2 only					1	1	1	1	2	2	2	2
Isy1	Pre-mRNA-splicing factor ISY1 homolog	Q69ZQ2	4.56	32989	WT1 only	WT2 only					1	1	1	1	1	1	1	1
Puf60	Poly(U)-binding-splicing factor PUF60	Q3UEB3	5.67	60248	WT1 only	WT2 only					2	2	2	2	1	1	1	1
Plrg1	Pleiotropic regulator 1	Q922V4	8.77	56937	WT1 only	WT2 only					2	2	2	2	1	1	1	1
RNA-binding																		
Fxr1	Fragile X mental retardation syndrome-related protein 1	Q61584	24.67	76221	WT1 only	WT2 only					8	9	8	8.68	10	10	9	9.63
Fxr2	Uncharacterized protein (Fragment)	Q3TA75	14.2	70528	WT1 only	WT2 only					4	5	4	4.32	4	5	4	4.3
Fmr1	Synaptic functional regulator FMR1	P35922	3.58	68989	WT1 only	WT2 only					1	1	1	1	2	2	1	1.07
Csde1	Cold shock domain-containing protein E1	Q91W50	4.26	88790	WT1 only	WT2 only					3	3	3	3	3	4	4	4
Mex3d	RNA-binding protein MEX3D	Q3UE17	17.88	65329	WT1 only	WT2 only					5	5	5	5	2	2	2	2
Eprs	Bifunctional glutamate/proline--tRNA ligase	Q8CGC7	2.98	170079	WT1 only	WT2 only					3	3	3	3	1	1	1	1
Vars	Valine--tRNA ligase	Q9Z1Q9	14.57	140215	WT1 only	WT2 only					12	14	14	14	6	7	7	7
Dars	Aspartate--tRNA ligase, cytoplasmic	Q922B2	8.58	57147	WT1 only	WT2 only					3	3	3	3	1	1	1	1
Lars	Leucine--tRNA ligase, cytoplasmic	Q8BMJ2	0.76	134192	WT1 only	WT2 only					1	1	1	1	1	2	2	2
Ylpm1	YLP motif-containing protein 1	D3YWX2	3.04	241050	WT1 only	WT2 only					2	2	2	2	4	4	4	4
Tarbp2	RISC-loading complex subunit TARBP2	P97473	7.4	38841	WT1 only	WT2 only					1	1	1	1	1	1	1	1
Dnaja4	DnaJ homolog subfamily A member 4	Q9JMC3	9.07	44901	WT1 only	WT2 only					3	4	4	4	2	3	3	3
Dnajb6	DnaJ homolog subfamily B member 6	O54946	6.58	39807	WT1 only	WT2 only					1	1	1	1	2	2	2	2
Dnaja2	DnaJ homolog subfamily A member 2	Q9QYJ0	8.5	45745	WT1 only	WT2 only					2	2	2	2	1	1	1	1
Igf2bp1	Insulin-like growth factor 2 mRNA-binding protein 1	O88477	4.68	63450	WT1 only	WT2 only					1	1	1	1	1	1	1	1
Stau1	Double-stranded RNA-binding protein Staufen homolog 1	Q92108	5.34	53924	WT1 only	WT2 only					2	2	2	2	1	1	1	1
Uri1	Unconventional prefoldin RPB5 interactor	Q3TLD5	4.9	59084	WT1 only	WT2 only					1	1	1	1	1	1	1	1
Mrto4	mRNA turnover protein 4 homolog	Q9D0I8	6.28	27545	WT1 only	WT2 only					1	1	1	1	1	1	1	1
Zfr	Zinc finger RNA-binding protein	O88532	8.29	116858	WT1 only	WT2 only					6	6	6	6	4	4	4	4
Rpl7	60S ribosomal protein L7	P14148	21.85	31419	WT1 only	WT2 only					6	6	6	6	6	6	6	6
Rpl7a	60S ribosomal protein L7a	P12970	12.41	29976	WT1 only	WT2 only					2	2	2	2	3	3	3	3
Rps24	40S ribosomal protein S24	P62849	18.05	15423	WT1 only	WT2 only					2	2	2	2	1	1	1	1
Rps15	40S ribosomal protein S15	P62843	24.83	17040	WT1 only	WT2 only					1	1	1	1	1	1	1	1
Rpl34	60S ribosomal protein L34	Q9D1R9	6.84	13292	WT1 only	WT2 only					1	1	1	1	1	1	1	1
Rpl38	60S ribosomal protein L38	Q9JJI8	14.29	8203	WT1 only	WT2 only					1	2	2	2	1	1	1	1
Alyref	THO complex subunit 4	O08583	14.51	26939	WT1 only	WT2 only					2	2	2	2	1	1	1	1
Nxf1	Nuclear RNA export factor 1	Q99JX7	1.94	70300	WT1 only	WT2 only					1	2	2	2	1	1	1	1
Larp4b	La-related protein 4B	Q6A0A2	5.94	81627	WT1 only	WT2 only					3	4	4	4	1	1	1	1
Exosc4	Exosome complex component RRP41	Q921I9	4.9	26250	WT1 only	WT2 only					1	1	1	1	1	1	1	1
Ddx6	Probable ATP-dependent RNA helicase DDX6	P54823	10.77	54191	WT1 only	WT2 only					4	4	4	4	4	4	4	4
Wtap	Pre-mRNA-splicing regulator WTAP	Q9ER69	9.34	44176	WT1 only	WT2 only					2	2	2	2	3	3	3	3
Atxn2l	Ataxin-2-like protein	Q3TGG2	7.24	105445	11.00	9.00	1	1	0	0.25	6	8	1	2.75	4	6	1	2.25
Dazap1	DAZ-associated protein 1	Q9JII5	7.64	43214	WT1 only	WT2 only					2	2	2	2	1	1	1	1
Fip1l1	Pre-mRNA 3'-end-processing factor FIP1	Q9D824	5.68	64958	WT1 only	WT2 only					1	1	1	1	1	1	1	1
Metabolism																		
Ndufa13	NADH dehydrogenase [ubiquinone] 1 alpha subcomplex subunit 13	Q9ERS2	6.25	16860	WT1 only	WT2 only					1	1	1	1	1	1	1	1
Ndufs1	NADH-ubiquinone oxidoreductase 75 kDa subunit, mitochondrial	Q91VD9	5.5	79776	WT1 only	WT2 only					3	3	3	3	2	2	2	2
Ndufv2	NADH dehydrogenase [ubiquinone] flavoprotein 2, mitochondrial	Q9D6J6	4.44	27285	WT1 only	WT2 only					1	1	1	1	1	1	1	1
Mrpl41	39S ribosomal protein L41, mitochondrial	Q9CQN7	8.89	15261	WT1 only	WT2 only					1	1	1	1	1	1	1	1
Gapdhs	Glyceraldehyde-3-phosphate dehydrogenase, testis-specific	Q64467	22.5	47656	WT1 only	WT2 only					6	10	9	9.63	4	4	3	3.63
Chchd3	MICOS complex subunit Mic19	Q9CRB9	10.13	26334	WT1 only	WT2 only					1	1	1	1	2	2	2	2
Immt	MICOS complex subunit Mic60	Q8CAQ8	15.19	83900	WT1 only	WT2 only					5	5	5	5	7	7	7	7
Pask	PAS domain-containing serine/threonine-protein kinase	Q8CEE6	7.16	151249	9.00	8.00	1	1	1	1	6	9	9	9	6	8	8	8
Pgk2	Phosphoglycerate kinase 2	P09041	6.71	44852	WT1 only	WT2 only					2	2	2	2	1	1	1	1
Dhx30	Putative ATP-dependent RNA helicase DHX30 (Fragment)	A0A0G2JEN9	75	1502	WT1 only	WT2 only					1	1	1	1	1	1	1	1
Atad3	ATPase family AAA domain-containing protein 3	Q925I1	1.35	66742	WT1 only	WT2 only					1	1	1	1	1	1	1	1
Ldha	L-lactate dehydrogenase A chain	P06151	14.46	36498	9.41	12.63	2	4	0	0.27	4	10	2	2.54	5	9	3	3.41
Mpc2	Mitochondrial pyruvate carrier 2	Q9D023	14.96	14285	WT1 only	WT2 only					1	1	1	1	2	2	2	2
Pdha1	Pyruvate dehydrogenase E1 component subunit alpha, somatic form, mitochondrial	P35486	2.56	43232	WT1 only	WT2 only					1	1	1	1	1	1	1	1
Pgam2	Phosphoglycerate mutase 2	O70250	4.74	28827	WT1 only	WT2 only					1	1	1	1	1	1	1	1
Gsto2	Glutathione S-transferase omega-2	Q8K2Q2	12.9	28599	WT1 only	WT2 only					2	2	2	2	2	2	2	2
Me1	NADP-dependent malic enzyme	P06801	3.15	63953	WT1 only	WT2 only					1	1	1	1	1	1	1	1
Tsta3	GDP-L-fucose synthase	P23591	3.74	35878	WT1 only	WT2 only					1	1	1	1	1	1	1	1

Table S3 (related to Figure 6C)

List of proteins identified following Nut immunoprecipitation from *WT* round/elongating spermatids and their *Nut KO* counterpart. The identified proteins belonging to the indicated functional categories are shown and highlighted.

Pep: number of identified peptides; SC: Spectral Counts; SSC: Specific Spectral Counts; WSC: Weighted Spectral Counts.

The colour-code is as follows:

- Classical contaminant

- Identified with 1 peptide but with SC and SSC >= 2
- Identified with several peptides but with SSC = 1
- Identified with 1 peptide and SC = 1
- Protein with SSC = 0

- Identified only in *WT* sample with WSC >= 5 or enriched at least 10 times in *WT* sample compared to *Nut* KO sample
- Identified only in *WT* sample with WSC >= 3 or enriched at least 5 times in *WT* sample compared to *Nut* KO sample

Shiota_Table S4 (related to Fig. 6D)

No	Modifications	Replications	Normalized peak area			Average normalized peak area		
			Nut	p300	Nut+p300	Nut	p300	Nut+p300
1	H3K9ac	1	1.38E+08	5.66E+09	2.18E+10	1.97E+08	5.93E+09	2.21E+10
		2	2.56E+08	6.19E+09	2.24E+10			
2	H3K14ac	1	1.70E+08	9.99E+09	2.69E+10	2.29E+08	9.90E+09	2.88E+10
		2	2.88E+08	9.81E+09	3.08E+10			
3	H3K18ac	1	2.28E+08	4.72E+10	1.18E+11	2.19E+08	5.42E+10	1.16E+11
		2	2.11E+08	6.11E+10	1.14E+11			
4	H3K23ac	1	1.50E+08	3.01E+10	9.16E+10	1.47E+08	3.13E+10	8.89E+10
		2	1.44E+08	3.26E+10	8.62E+10			
5	H3K27ac	1	1.48E+08	3.94E+10	7.47E+10	1.48E+08	4.01E+10	7.01E+10
		2	1.48E+08	4.08E+10	6.55E+10			
6	H3K36ac	1	2.01E+07	6.81E+08	1.97E+09	2.07E+07	8.04E+08	2.23E+09
		2	2.13E+07	9.26E+08	2.50E+09			
7	H3K56ac	1	5.49E+07	2.55E+08	2.91E+08	4.49E+07	2.20E+08	2.55E+08
		2	3.49E+07	1.85E+08	2.19E+08			
8	H3K79ac	1	6.58E+07	7.10E+07	9.94E+07	6.77E+07	7.04E+07	8.97E+07
		2	6.97E+07	6.99E+07	8.00E+07			
9	H3K122ac	1	1.91E+07	3.56E+08	7.80E+08	1.90E+07	3.45E+08	7.34E+08
		2	1.89E+07	3.33E+08	6.89E+08			
10	H4K5ac	1	7.81E+07	1.10E+10	3.93E+10	7.77E+07	1.03E+10	4.76E+10
		2	7.73E+07	9.56E+09	5.59E+10			
11	H4K8ac	1	8.31E+07	1.21E+10	4.10E+10	8.30E+07	1.14E+10	5.01E+10
		2	8.30E+07	1.07E+10	5.92E+10			
12	H4K12ac	1	5.70E+07	7.21E+09	2.18E+10	5.49E+07	6.79E+09	2.52E+10
		2	5.28E+07	6.37E+09	2.87E+10			
13	H4K16ac	1	1.29E+07	2.01E+09	8.20E+09	1.19E+07	1.78E+09	8.80E+09
		2	1.09E+07	1.54E+09	9.40E+09			
14	H4K31ac	1	6.51E+07	1.62E+09	2.52E+09	5.77E+07	1.41E+09	2.71E+09
		2	5.03E+07	1.21E+09	2.90E+09			
15	H4K77ac	1	1.92E+07	4.36E+07	7.17E+07	1.95E+07	4.35E+07	6.83E+07
		2	1.97E+07	4.35E+07	6.49E+07			
16	H4K79ac	1	5.79E+06	1.09E+07	1.89E+07	5.43E+06	1.07E+07	1.56E+07
		2	5.08E+06	1.05E+07	1.23E+07			
17	H4K91ac	1	1.46E+07	2.73E+07	7.16E+07	1.56E+07	2.06E+07	6.54E+07
		2	1.67E+07	1.38E+07	5.92E+07			

Table S4 (related to Figure 6D)

Identified site-specific acetylation of histones incubated with p300 and the p300-interacting domain of NUT (see Table S5 for details).

All the identified peptides with a Mascot score above 20 were manually verified according to the rules described previously (Chen et al., 2005).

Shiota_Table S5 (related to Fig. 6D)

Site	Peptide	Peak area					
		Nut-1	Nut-2	p300-1	p300-2	Nut+p300-1	Nut+p300-2
H3K9ac	K(ac)STGGK(ac)APR	1.38E+08	2.28E+08	7.08E+09	5.75E+09	2.25E+10	1.79E+10
	SUM	1.38E+08	2.28E+08	7.08E+09	5.75E+09	2.25E+10	1.79E+10
H3K14ac	K(ac)STGGK(ac)APR	1.38E+08	2.28E+08	7.08E+09	5.75E+09	2.25E+10	1.79E+10
	KSTGGK(ac)APR	1.78E+07	1.59E+07	1.67E+09	3.23E+08	1.31E+08	4.40E+08
	STGGK(ac)APR	1.48E+07	1.27E+07	3.74E+09	3.04E+09	5.07E+09	6.28E+09
	SUM	1.70E+08	2.56E+08	1.25E+10	9.12E+09	2.77E+10	2.46E+10
H3K18ac	K(ac)QLATK(ac)AAR	1.46E+08	1.24E+08	3.47E+10	2.65E+10	9.25E+10	6.97E+10
	K(ac)QLATK	8.14E+07	6.39E+07	2.42E+10	3.03E+10	2.88E+10	2.16E+10
	SUM	2.28E+08	1.88E+08	5.90E+10	5.69E+10	1.21E+11	9.13E+10
H3K23ac	K(ac)QLATK(ac)AAR	1.46E+08	1.24E+08	3.47E+10	2.65E+10	9.19E+10	6.73E+10
	KQLATK(ac)AAR	NA	NA	1.69E+09	2.93E+09	1.85E+09	1.20E+09
	QLATK(ac)AAR	3.59E+06	4.37E+06	1.20E+09	8.33E+08	6.03E+08	4.83E+08
	SUM	1.50E+08	1.28E+08	3.76E+10	3.03E+10	9.44E+10	6.90E+10
H3K27ac	K(ac)SAPATGGVK	1.46E+08	1.31E+08	4.89E+10	3.76E+10	7.55E+10	5.12E+10
	K(ac)SAPATGGVK(me)	NA	NA	2.40E+07	1.96E+07	3.68E+07	3.32E+07
	K(ac)SAPATGGVK(ac)KPHR	1.86E+06	1.53E+06	2.69E+08	3.60E+08	1.42E+09	1.18E+09
	SUM	1.48E+08	1.32E+08	4.92E+10	3.80E+10	7.70E+10	5.24E+10
H3K36ac	K(ac)SAPATGGVK(ac)KPHR	1.86E+06	1.53E+06	2.69E+08	3.60E+08	1.42E+09	1.18E+09
	SAPATGGVK(ac)KPHR	9.63E+06	9.63E+06	4.60E+08	4.20E+08	3.85E+08	3.67E+08
	KSAPATGGVK(ac)KPHR	8.66E+06	7.81E+06	1.23E+08	7.66E+07	2.26E+08	4.52E+08
	SUM	2.01E+07	1.90E+07	8.52E+08	8.57E+08	2.03E+09	2.00E+09
H3K56ac	RYQK(ac)STELLIR	5.90E+06	4.48E+06	5.92E+07	3.32E+07	4.90E+07	3.10E+07
	YQK(ac)STELLIR	4.90E+07	2.66E+07	2.60E+08	1.39E+08	2.50E+08	1.44E+08
	SUM	5.49E+07	3.10E+07	3.19E+08	1.72E+08	2.99E+08	1.75E+08
H3K79ac	EIAQDFK(ac)TDLR	6.58E+07	6.20E+07	8.87E+07	6.50E+07	1.02E+08	6.40E+07
	SUM	6.58E+07	6.20E+07	8.87E+07	6.50E+07	1.02E+08	6.40E+07
H3K122ac	RVTIM(o)PK(ac)DIQLAR	7.99E+05	3.92E+05	9.54E+07	1.03E+08	2.68E+08	1.94E+08
	VTIM(o)PK(ac)DIQLAR	1.83E+07	1.65E+07	3.50E+08	2.07E+08	5.36E+08	3.57E+08
	SUM	1.91E+07	1.69E+07	4.45E+08	3.10E+08	8.03E+08	5.51E+08
H4K5ac	GK(ac)GGK(ac)GLGK	4.60E+07	3.97E+07	7.49E+09	5.15E+09	2.15E+10	2.49E+10
	GK(ac)GGK(ac)GLGK(ac)GGAK	2.08E+07	2.08E+07	4.14E+09	2.53E+09	1.17E+10	1.34E+10
	GK(ac)GGK(ac)GLGK(ac)GGAK(ac)R	1.14E+07	8.33E+06	2.12E+09	1.20E+09	7.29E+09	6.39E+09
	SUM	7.81E+07	6.88E+07	1.37E+10	8.89E+09	4.04E+10	4.47E+10
H4K8ac	GKGGK(ac)GLGK	4.96E+06	5.03E+06	1.24E+09	9.36E+08	1.26E+09	2.25E+09
	GK(ac)GGK(ac)GLGK	4.60E+07	3.97E+07	7.49E+09	5.15E+09	2.15E+10	2.49E+10
	GK(ac)GGK(ac)GLGK(ac)GGAK	2.08E+07	2.08E+07	4.14E+09	2.53E+09	1.17E+10	1.34E+10
	GK(ac)GGK(ac)GLGK(ac)GGAK(ac)R	1.14E+07	8.33E+06	2.12E+09	1.20E+09	7.29E+09	6.39E+09
	GGK(ac)GLGK(ac)GGAK(ac)R	NA	NA	1.49E+08	8.42E+07	5.23E+08	4.26E+08
	SUM	8.31E+07	7.38E+07	1.51E+10	9.91E+09	4.22E+10	4.74E+10
H4K12ac	GK(ac)GGK(ac)GLGK(ac)GGAK	2.08E+07	2.08E+07	4.14E+09	2.53E+09	1.17E+10	1.34E+10
	GK(ac)GGK(ac)GLGK(ac)GGAK(ac)R	1.14E+07	8.33E+06	2.12E+09	1.20E+09	7.29E+09	6.39E+09
	GGK(ac)GLGK(ac)GGAK(ac)R	NA	NA	1.49E+08	8.42E+07	5.23E+08	4.26E+08
	GLGK(ac)GGAK	2.32E+07	1.65E+07	2.36E+09	1.96E+09	2.36E+09	2.01E+09
	GLGK(ac)GGAK(ac)R	1.55E+06	1.41E+06	2.47E+08	1.50E+08	6.35E+08	7.02E+08
	SUM	5.70E+07	4.70E+07	9.01E+09	5.92E+09	2.25E+10	2.29E+10
H4K16ac	GK(ac)GGK(ac)GLGK(ac)GGAK(ac)R	1.14E+07	8.33E+06	2.12E+09	1.20E+09	7.29E+09	6.39E+09
	GGK(ac)GLGK(ac)GGAK(ac)R	NA	NA	1.49E+08	8.42E+07	5.23E+08	4.26E+08
	GLGK(ac)GGAK(ac)R	1.55E+06	1.41E+06	2.47E+08	1.50E+08	6.35E+08	7.02E+08
	SUM	1.29E+07	9.74E+06	2.51E+09	1.43E+09	8.45E+09	7.52E+09
H4K31ac	DNIQGITK(ac)PAIR	6.51E+07	4.47E+07	2.03E+09	1.12E+09	2.60E+09	2.32E+09
	SUM	6.51E+07	4.47E+07	2.03E+09	1.12E+09	2.60E+09	2.32E+09
H4K77ac	DAVTYTEHAK(ac)R	1.92E+07	1.76E+07	5.45E+07	4.05E+07	7.38E+07	5.19E+07
	SUM	1.92E+07	1.76E+07	5.45E+07	4.05E+07	7.38E+07	5.19E+07
H4K79ac	K(ac)TVTAM(o)DVVYALK	5.79E+06	4.52E+06	1.37E+07	9.81E+06	1.94E+07	9.83E+06
	SUM	5.79E+06	4.52E+06	1.37E+07	9.81E+06	1.94E+07	9.83E+06
H4K91ac	KTVTAM(o)DVVYALK(ac)R	8.32E+06	8.85E+06	1.73E+07	5.34E+06	2.94E+07	1.84E+07
	TVTAM(o)DVVYALK(ac)R	6.27E+06	5.98E+06	1.68E+07	7.53E+06	4.44E+07	2.89E+07
	SUM	1.46E+07	1.48E+07	3.41E+07	1.29E+07	7.37E+07	4.73E+07
Normalization							
	Peptide	NUT-1	NUT-2	p300-1	p300-2	Nut+p300-1	Nut+p300-2
H3	YRPGTVALR	8.63E+10	8.07E+10	1.03E+11	7.60E+10	8.68E+10	6.33E+10
	STELLIR	2.33E+11	2.12E+11	2.87E+11	2.15E+11	2.39E+11	1.82E+11
	EIAQDFK	1.19E+11	1.04E+11	1.36E+11	1.13E+11	1.27E+11	7.27E+10
H4	DNIQGITKPAIR	1.01E+11	8.26E+10	1.35E+11	9.24E+10	1.00E+11	9.03E+10
	ISGLIYEETR	2.55E+11	2.27E+11	3.29E+11	2.39E+11	2.67E+11	2.28E+11
Average		1.59E+11	1.41E+11	1.98E+11	1.47E+11	1.64E+11	1.27E+11

Table S5 (related to Figure 6D)

Detailed quantitative analysis of site-specific histone acetylation after octamer incubation with p300 and the p300-interacting domain of NUT shown in Table S4.